Contents lists available at GrowingScience

Current Chemistry Letters

homepage: www.GrowingScience.com

Microwave-assisted one-pot lemon-juice-catalyzed synthesis of trifluoromethyl coumarin-based 4*H*-Pyran hybrids and their antimicrobial evaluation

Chaitanya K. Shah[a], Rajesh H. Vekariya[b], Jinal A. Gajjar[c], Dhanji P. Rajani[d] and Anil Kumar[a*]

[a]*SunRise University, Bagar Rajput, Alwar, Rajasthan, 301028, India*
[b]*Gujarat Fluorochemicals Ltd., Survey No. 16/3, 26-27, Village Rajitnagar, Taluka Ghoghamba, Dist. Panchmahal, Gujarat-389380, India*
[c]*Jeel Goswami College of Science & Research, Monark University, Vahelal - Dahegam road, Naroda, Ahmedabad, Gujarat-38233, India*
[d]*Microcare Laboratory and TRC, Surat, Gujarat, India-395003, India*

C H R O N I C L E

Article history:
Received March 15, 2026
Received in revised form
June 19, 2026
Accepted September 1, 2026
Available online
September 1, 2026

Keywords:
Trifluoromethyl coumarins
Pyrano[3,2-g]chromenes
Microwave-assisted synthesis
Lemon juice catalyst
Green chemistry
Multicomponent reaction
Fluorinated heterocycles
Antimicrobial activity
Antifungal activity
Structure-activity relationship (SAR)

A B S T R A C T

A green and efficient microwave-assisted one-pot multicomponent strategy was developed for the synthesis of novel trifluoromethyl coumarin-based 4*H*-pyran hybrids using freshly extracted lemon juice as a natural biocatalyst. The reaction of 7-hydroxy-4-(trifluoromethyl)coumarin, malononitrile, and various aromatic/heteroaromatic aldehydes in an ethanol:water (1:1) medium under microwave irradiation afforded a series of 2-amino-8-oxo-4-aryl-6-(trifluoromethyl)-4,8-dihydropyrano[3,2-*g*]chromene-3-carbonitrile derivatives **(4a-p)** in excellent yields (86-94%) within 4-8 min. Optimization studies identified lemon juice (5 mL) under 300 W microwave irradiation as the most effective and environmentally benign catalytic system. Kinetic studies revealed pseudo-first-order behaviour, confirming the high efficiency of the lemon juice-microwave protocol. All synthesized compounds were characterized by FT-IR, ^{1}H-NMR, ^{13}C-NMR, ^{19}F-NMR, mass spectrometry, and elemental analysis. Biological screening demonstrated promising antibacterial and antifungal activities, with compounds **(4l)**, **(4m)**, and **(4i)** exhibiting the highest potency and MIC values comparable to standard drugs against selected microbial strains. Structure-activity relationship studies revealed that electron-withdrawing substituents on the aryl ring significantly enhanced antimicrobial activity. Overall, this sustainable methodology offers rapid access to biologically relevant fluorinated heterocycles and identifies promising lead molecules for the development of new antimicrobial agents.

2026 by the authors; licensee Growing Science, Canada.

1. Introduction

The development of environmentally benign synthetic methodologies has become a central objective of modern organic chemistry owing to increasing environmental concerns and the growing demand for sustainable chemical processes.[1] Green chemistry principles advocate the use of renewable resources, non-toxic catalysts, atom-economic reactions, and waste minimization strategies.[2] In this context, one-pot multicomponent reactions (MCRs) have emerged as powerful synthetic tools for the rapid generation of molecular complexity from simple starting materials. MCRs offer significant advantages such as operational simplicity, high atom economy, reduced reaction times, easy product isolation, and decreased solvent consumption, making them attractive approaches for the synthesis of biologically important heterocyclic compounds.[3]

Heterocyclic molecules constitute a major class of compounds in medicinal chemistry, with oxygen-containing heterocycles occupying a prominent position due to their broad spectrum of biological activities.[4] Among them, 4*H*-pyran derivatives and their fused analogues have attracted considerable attention because of their diverse pharmacological properties.[5] 4*H*-Pyrans constitute an important class of oxygen-containing heterocyclic compounds and serve as key structural motifs in numerous naturally occurring products **(Fig. 1)**.[6,7] Numerous studies have reported that 4*H*-pyrans exhibit significant anticancer,[8] antimicrobial,[9] antiviral,[10] anti-inflammatory,[11] antioxidant,[12] antitubercular,[13] and neuroprotective[14] activities. Furthermore, these compounds have shown therapeutic potential against neurodegenerative

* Corresponding author
E-mail address anil1910alw@gmail.com (A. Kumar)
© 2026 by the authors; licensee Growing Science, Canada
doi: 10.5267/j.ccl.2026.9.002

disorders such as Alzheimer's disease,[15] Parkinson's disease,[16] and Huntington's disease.[17] In addition to their pharmaceutical importance, 2-amino-4*H*-pyran derivatives have found applications as photoactive materials, pigments, optical brighteners, and biodegradable agrochemicals.[18,19]

Coumarins represent another privileged class of oxygen-containing heterocycles widely distributed in nature and extensively explored in medicinal chemistry.[20] Coumarin derivatives possess a broad range of biological activities,[21] including antimicrobial,[22,23] antifungal,[24,25] antiviral,[26] anticancer,[27] anticoagulant,[28] antioxidant,[29] antimalarial,[30] antitubercular,[31] and anti-inflammatory[32] properties. Structural modification of the coumarin nucleus has proven to be an effective strategy for enhancing biological potency and improving physicochemical properties.[33] In particular, the incorporation of fluorinated functionalities into biologically active molecules has become a powerful approach in contemporary drug design.[34] Fluorine-containing compounds frequently exhibit enhanced metabolic stability, lipophilicity, membrane permeability, and target-binding affinity compared to their non-fluorinated counterparts.[35]

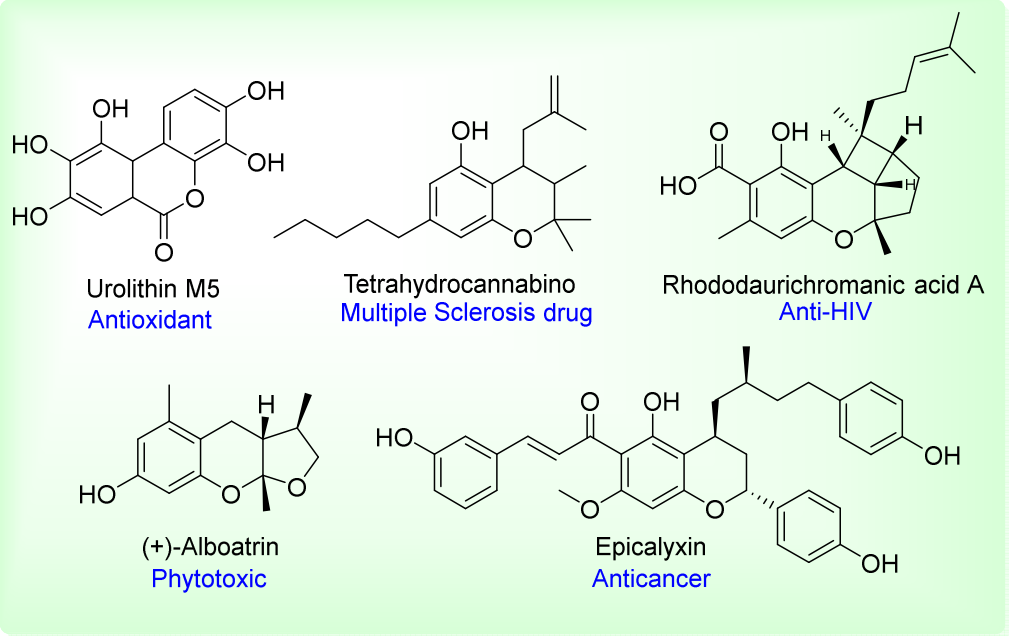

Fig. 1. Natural product containing benzopyran/chromene derivatives

Among fluorinated substituents, the trifluoromethyl (-CF_3) group is one of the most valuable pharmacophores in medicinal and agrochemical chemistry.[36,37] The strong electron-withdrawing nature and unique physicochemical characteristics of the trifluoromethyl group significantly influence molecular conformation, biological activity, and pharmacokinetic behavior.[38] Consequently, trifluoromethyl-substituted coumarins have emerged as promising scaffolds exhibiting potent antimicrobial, antifungal, anticancer, and enzyme inhibitory activities.[39] The combination of a trifluoromethyl-containing coumarin moiety with other biologically active heterocyclic frameworks thus represents an attractive strategy for the development of novel bioactive molecules with enhanced therapeutic potential.[40]

Molecular hybridization has recently gained significant importance as an effective drug-design approach for generating multifunctional compounds by combining two or more pharmacologically relevant scaffolds into a single molecular framework.[41] In this regard, hybrid molecules containing both coumarin and 4*H*-pyran motifs are expected to exhibit synergistic biological effects arising from the contribution of each pharmacophore.42,43 Despite the remarkable biological significance of these heterocyclic systems, reports describing the synthesis of trifluoromethyl coumarin-linked 4*H*-pyran derivatives using environmentally sustainable methodologies remain limited.[44]

Simultaneously, there is growing interest in replacing conventional catalysts with naturally derived catalytic systems.[45] Fruit extracts rich in naturally occurring organic acids have emerged as inexpensive, biodegradable, and renewable alternatives to synthetic catalysts.[46] Among them, lemon (*Citrus limon*) juice is particularly attractive owing to its high content of citric acid, ascorbic acid, malic acid, and other naturally occurring acidic constituents.[47] These components provide an effective acidic medium capable of promoting various organic transformations under mild conditions.[48] The use of lemon juice as a bio-catalyst offers several advantages, including low cost, easy availability, non-toxicity, biodegradability, and compliance with green chemistry principles.[49]

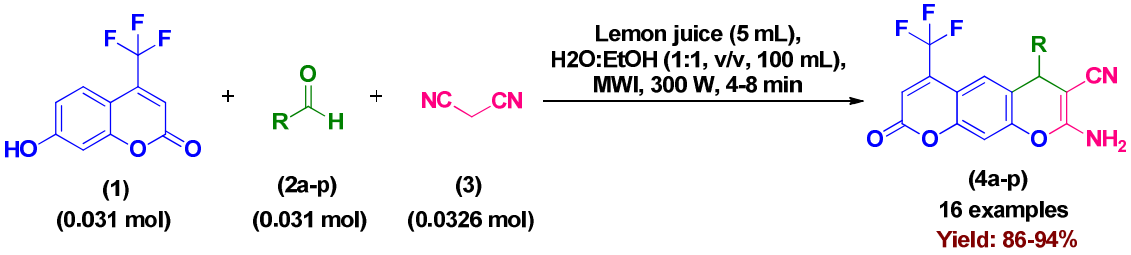

Entry	Aldehyde Code	R-Substituent	Product Code	Yield
1	2a	Phenyl	4a	89
2	2b	4-Methoxyphenyl	4b	92
3	2c	4-Methylphenyl	4c	88
4	2d	2-Methylphenyl	4d	91
5	2e	4-Dimethylaminophenyl	4e	89
6	2f	3-Methoxyphenyl	4f	86
7	2g	4-Chlorophenyl	4g	92
8	2h	2-Chlorophenyl	4h	88
9	2i	4-Bromophenyl	4i	94
10	2j	2,5-Dimethoxyphenyl	4j	86
11	2k	3,4,5-Trimethoxyphenyl	4k	88
12	2l	4-Fluorophenyl	4l	93
13	2m	4-Nitrophenyl	4m	94
14	2n	3-Pyridyl	4n	88
15	2o	2-Furyl	4o	86
16	2p	2-Thienyl	4p	87

Scheme 1. Synthesis of novel trifluoromethyl coumarin-based 4*H*-pyran derivatives **(4a-p)**

Inspired by the biological importance of 4*H*-pyrans and trifluoromethyl-substituted coumarins, and motivated by the need for sustainable synthetic methodologies, we report herein a facile one-pot multicomponent synthesis of novel trifluoromethyl coumarin-based 4*H*-pyran derivatives using freshly extracted lemon juice as a natural acid catalyst **(Scheme 1)**. The developed protocol provides an environmentally friendly, operationally simple, and efficient route for the construction of structurally diverse heterocyclic hybrids under mild reaction conditions. Furthermore, the synthesized compounds were evaluated for their antimicrobial and antifungal activities against selected pathogenic microorganisms to investigate the influence of the combined 4*H*-pyran and trifluoromethyl coumarin pharmacophores on biological activity. The results demonstrate the potential of this green synthetic strategy for generating novel fluorinated heterocyclic hybrids with promising antimicrobial and antifungal properties, thereby contributing to the development of sustainable approaches in medicinal and synthetic organic chemistry.

2. Material and methods

2.1. Chemicals and reagents

All chemicals, reagents, and solvents employed in the present study were of analytical reagent (AR) grade and were purchased from commercial suppliers. 7-Hydroxy-4-(trifluoromethyl)-2*H*-chromen-2-one was synthesized from resorcinol and 4,4,4-trifluoro ethyl acetoacetate using a literature-reported procedure involving iodine (5 mol%) as a catalyst in toluene at 80 °C.[50] Aromatic and heteroaromatic aldehydes, malononitrile, citric acid, *para*-toluenesulfonic acid (*p*-TSA), acetic acid, and other reagents were obtained from Sigma-Aldrich, Merck, Spectrochem, or SRL Chemicals and used without further purification unless otherwise stated. Fresh lemon juice was extracted from ripe lemons immediately before use and filtered to remove insoluble materials. Ethanol and distilled water were used as reaction media throughout the study. The progress of the reactions was monitored by thin-layer chromatography (TLC) on pre-coated silica gel 60 F254 aluminum sheets (Merck), and the spots were visualized under ultraviolet light (254 and 365 nm).

2.2. Instrumentation

Melting points were determined on an Optimelt MPA 100 melting point apparatus and are reported uncorrected. Fourier-transform infrared (FT-IR) spectra were recorded on a PerkinElmer FT-IR spectrometer using KBr pellets, and absorption frequencies are reported in cm^{-1}. Proton nuclear magnetic resonance (^{1}H-NMR) spectra were recorded on a Bruker Avance 400 MHz spectrometer using DMSO-d_6 as solvent and tetramethylsilane (TMS) as the internal standard. Carbon-13 nuclear magnetic resonance (^{13}C-NMR) spectra were obtained on a Bruker Avance 100 MHz spectrometer using DMSO-d_6 as solvent. Fluorine-19 nuclear magnetic resonance (^{19}F-NMR) spectra were recorded at 376 MHz using DMSO-d_6 as solvent. Chemical shifts (δ) are reported in parts per million (ppm), and coupling constants (*J*) are expressed in Hertz (Hz). Mass spectral analyses were performed on an Advion Expression Compact Mass Spectrometer (CMS, USA) equipped with an electrospray ionization (ESI) source using acetone as the mobile phase. Elemental analyses (CHN) were carried out using a CHNS elemental analyzer, and the obtained results were within ±0.4% of the theoretical values. Microwave-assisted

reactions were conducted in a laboratory microwave reactor (Domestic modified microwave) operating at variable power outputs up to 500 W. UV-visible absorption spectra for kinetic studies were recorded on a UV-visible spectrophotometer using quartz cuvettes of 1 cm path length over the wavelength range of 250-600 nm at ambient temperature.

2.3. General procedure for the synthesis of 2-amino-8-oxo-4-aryl-6-(trifluoromethyl)-4,8-dihydropyrano[3,2-g]chromene-3-carbonitrile

A mixture of 7-hydroxy-4-(trifluoromethyl)coumarin (7.13 g, 0.031 mol), corresponding benzaldehyde (0.031 mol), and malononitrile (2.15 g, 0.0326 mol) was suspended in a ethanol:water mixture (1:1, v/v, 100 mL) in a 250 mL microwave-compatible reaction vessel along with reflux condenser. Freshly extracted lemon juice (5 mL) was added as a natural acid catalyst, and the reaction mixture was stirred at room temperature for 5 min. The reaction mixture was then irradiated under microwave conditions at 300 W for 5-8 min. The progress of the reaction was monitored by TLC using ethyl acetate: *n*-hexane (3:7) as the developing solvent. After completion of the reaction, the mixture was allowed to cool to room temperature and poured into 150 mL of ice-cold water. The resulting yellow precipitate was collected by vacuum filtration, washed with cold water (2 × 25 mL), and dried under reduced pressure at 60 °C. The crude product was recrystallized from ethanol to afford pure 2-amino-8-oxo-4-aryl-6-(trifluoromethyl)-4,8-dihydropyrano[3,2-*g*]chromene-3-carbonitrile in excellent yield. Detailed spectroscopic data of **(4b-p)** were mentioned in supporting information file.

2-Amino-8-oxo-4-phenyl-6-(trifluoromethyl)-4,8-dihydropyrano[3,2-*g*]chromene-3-carbonitrile (4a)

Yield: 89%; Yellow crystalline solid; MP: 212-214 °C; IR (KBr) ν: 3362 (NH2), 2224 (CN), 1722 (C=C-C=O), 1623 (C=C), 1512, 1468, 1262, 1218, 1168 (CF_3), 1125, 1088 cm^{-1}; ^{1}H-NMR (400 MHz, DMSO-d_6, TMS) δ: 4.86 (s, 1H, pyran-H), 6.38 (s, 1H, Ar-H), 6.72 (s, 1H, coumarin-H), 7.02 (s, 2H, NH_2), 7.18-7.46 (m, 5H, Ar-H), 7.68 (s, 1H, Ar-H) ppm; ^{13}C-NMR (100 MHz, DMSO-d_6, TMS) δ: 36.4 (CH), 58.7 (C–CN), 112.3 (C–NH_2), 115.1 (Ar-C), 116.4 (Ar-C), 118.8 (C≡N), 122.4 (CF_3), 124.6 (Ar-C), 127.9 (Ar-C), 128.6 (Ar-C), 129.8 (Ar-C), 131.2 (Ar-C), 139.5 (Ar-C), 151.6 (Ar-C), 153.4 (Ar-C), 158.8 (Ar-C), 160.9 (Ar-C), 176.8 (C=O) ppm; ^{19}F-NMR (376 MHz, DMSO-d_6) δ: -62.360 (s, 3F, CF_3) ppm; ESI-MS *m/z* for ($C_{20}H_{11}F_3N_2O_3$) (384.07): 385.1 $(M+1)^+$; Elemental Analysis: Calculated for $C_{20}H_{11}F_3N_2O_3$ (384.31): C 62.51%, H 2.89%, N 14.83%; Found: C 62.48%, H 2.892%, N 14.86%.

2-Amino-4-(4-methoxyphenyl)-8-oxo-6-(trifluoromethyl)-4,8-dihydropyrano[3,2-*g*]chromene-3-carbonitrile (4b)

Yield: 91%; Pale yellow crystalline solid; MP: 218-220 °C; IR (KBr) ν: 3365 (NH_2), 2222 (CN), 1720 (C=C-C=O), 1621 (C=C), 1604, 1515, 1465, 1258 (Ar-OCH_3), 1216, 1170 (CF_3), 1128, 1085 cm^{-1}; ^{1}H-NMR (400 MHz, DMSO-d_6, TMS) δ: 3.65 (s, 3H, OCH_3), 4.61 (s, 1H, pyran-H), 6.34 (s, 1H, Ar-H), 6.47 (d, *J* = 8.12 Hz, 2H, Ar-H), 6.76 (s, 1H, coumarin-H), 6.91 (s, 2H, NH_2), 7.64 (s, 1H, Ar-H), 7.93 (d, *J* = 9.8 Hz, 2H, Ar-H) ppm; ^{13}C-NMR (100 MHz, DMSO-d_6, TMS) δ: 36.1 (CH), 55.4 (OCH_3), 58.5 (C–CN), 112.1 (C–NH_2), 114.2 (Ar-C), 115.0 (Ar-C), 116.5 (Ar-C), 118.7 (C≡N), 122.5 (CF_3), 124.4 (Ar-C), 128.3 (Ar-C), 129.6 (Ar-C), 131.1 (Ar-C), 151.5 (Ar-C), 153.2 (Ar-C), 158.7 (Ar-C), 159.8 (Ar-C), 160.8 (Ar-C), 176.7 (C=O) ppm; ^{19}F-NMR (376 MHz, DMSO-d_6) δ: -62.422 (s, 3F, CF_3) ppm; ESI-MS m/z for ($C_{21}H_{13}F_3N_2O_4$) (414.08): 415.2 $(M+1^+)$; Elemental Analysis: Calculated for $C_{21}H_{13}F_3N_2O_4$ (414.33): C 60.88%, H 3.16%, N 6.76%; Found: C 60.84%, H 3.18%, N 6.79%.

2-amino-8-oxo-4-(*p*-tolyl)-6-(trifluoromethyl)-4,8-dihydropyrano[3,2-*g*]chromene-3-carbonitrile (4c)

Yield: 90%; Yellow crystalline solid; MP: 216-218 °C; IR (KBr) ν: 3364 (NH_2), 2223 (CN), 1721 (C=C-C=O), 1622 (C=C), 1514, 1466, 1368 (CH_3), 1260, 1217, 1169 (CF_3), 1126, 1087 cm^{-1}; ^{1}H-NMR (400 MHz, DMSO-d_6, TMS) δ: 2.28 (s, 3H, CH_3), 4.64 (s, 1H, pyran-H), 6.37 (s, 1H, H-C=C), 7.06 (s, 2H, NH_2), 7.12 (d, *J* = 8.0 Hz, 2H, Ar-H), 7.18 (s, 1H, Ar-H), 7.26 (d, *J* = 8.0 Hz, 2H, Ar-H), 7.67 (s, 1H, Ar-H) ppm; ^{13}C-NMR (100 MHz, DMSO-d_6, TMS) δ: 20.9 (CH_3), 36.3 (CH), 58.6 (C–CN), 112.2 (C–NH_2), 115.0 (Ar-C), 116.3 (Ar-C), 118.8 (C≡N), 122.4 (CF_3), 124.5 (Ar-C), 127.6 (Ar-C), 129.1 (Ar-C), 129.8 (Ar-C), 131.2 (Ar-C), 136.7 (Ar-C), 151.5 (Ar-C), 153.3 (Ar-C), 158.8 (Ar-C), 160.8 (Ar-C), 176.8 (C=O) ppm; ^{19}F-NMR (376 MHz, DMSO-d_6) δ: -62.334 (s, 3F, CF_3) ppm; ESI-MS m/z for ($C_{21}H_{13}F_3N_2O_3$) (398.09): 399.2 $(M+1)^+$; Elemental Analysis: Calculated for $C_{21}H_{13}F_3N_2O_3$ (398.33): C 63.32%, H 3.29%, N 7.03%; Found: C 63.29%, H 3.31%, N 7.01%.

2-amino-8-oxo-4-(*o*-tolyl)-6-(trifluoromethyl)-4,8-dihydropyrano[3,2-*g*]chromene-3-carbonitrile (4d)

Yield: 88%; Yellow crystalline solid; MP: 209-211 °C; IR (KBr) ν: 3363 (NH_2), 2224 (CN), 1721 (C=C-C=O), 1622 (C=C), 1513, 1467, 1370 (CH_3), 1261, 1218, 1168 (CF_3), 1127, 1086 cm^{-1}; ^{1}H-NMR (400 MHz, DMSO-d_6, TMS) δ: 2.31 (s, 3H, CH_3), 4.71 (s, 1H, pyran-H), 6.39 (s, 1H, H-C=C), 7.04 (s, 2H, NH_2), 7.08-7.26 (m, 4H, Ar-H), 7.19 (s, 1H, Ar-H), 7.70 (s, 1H, Ar-H); ^{13}C-NMR (100 MHz, DMSO-d_6, TMS) δ: 19.6 (CH_3), 34.8 (CH), 58.4 (C–CN), 112.3 (C–NH_2), 115.1 (Ar-C), 116.4 (Ar-C), 118.8 (C≡N), 122.4 (CF_3), 124.6 (Ar-C), 126.8 (Ar-C), 127.5 (Ar-C), 129.2 (Ar-C), 130.4 (Ar-C), 131.1 (Ar-C), 136.2 (Ar-C), 137.9 (Ar-C), 151.6 (Ar-C), 153.4 (Ar-C), 158.8 (Ar-C), 160.9 (Ar-C), 176.8 (C=O) ppm; ^{19}F-NMR (376 MHz, DMSO-d_6) δ: -62.267 (s, 3F, CF_3) ppm; ESI-MS m/z for ($C_{21}H_{13}F_3N_2O_3$) (398.09): 399.2 $(M+1)^+$; Elemental Analysis: Calculated for $C_{21}H_{13}F_3N_2O_3$ (398.33): C 63.32%, H 3.29%, N 7.03%; Found: C 63.35%, H 3.27%, N 7.05%.

2-amino-4-(4-(dimethylamino)phenyl)-8-oxo-6-(trifluoromethyl)-4,8-dihydropyrano[3,2-*g*]chromene-3-carbonitrile (4e)

Yield: 93%; Orange-yellow crystalline solid; MP: 224-226 °C; IR (KBr) ν: 3366 (NH_2), 2221 (CN), 1720 (C=C-C=O), 1620 (C=C), 1608, 1518, 1464, 1342 ($N(CH_3)_2$), 1260, 1215, 1171 (CF_3), 1129, 1084 cm^{-1}; ^{1}H-NMR (400 MHz, DMSO-d_6, TMS) δ: 2.94 (s, 6H, $N(CH_3)_2$), 4.62 (s, 1H, pyran-H), 6.35 (s, 1H, H-C=C), 6.72 (d, *J* = 8.8 Hz, 2H, Ar-H), 7.09 (s, 2H, NH_2), 7.16 (s, 1H, Ar-H), 7.24 (d, *J* = 8.8 Hz, 2H, Ar-H), 7.65 (s, 1H, Ar-H) ppm; ^{13}C-NMR (100 MHz, DMSO-d_6, TMS) δ: 36.0 (CH), 40.3 ($N(CH_3)_2$), 58.4 (C–CN), 112.0 (C–NH_2), 112.8 (Ar-C), 114.6 (Ar-C), 116.5 (Ar-C), 118.7 (C≡N), 122.5 (CF_3), 124.3 (Ar-C), 127.8 (Ar-C), 129.4 (Ar-C), 131.0 (Ar-C), 150.2 (Ar-C), 151.4 (Ar-C), 153.1 (Ar-C), 158.6 (Ar-C), 160.7 (Ar-C), 176.6 (C=O) ppm; ^{19}F-NMR (376 MHz, DMSO-d_6) δ: -62.389 (s, 3F, CF_3) ppm; ESI-MS m/z for ($C_{22}H_{16}F_3N_3O_3$) (427.11): 428.2 $(M+1)^+$; Elemental Analysis: Calculated for $C_{22}H_{16}F_3N_3O_3$ (427.38): C 61.83%, H 3.77%, N 9.83%; Found: C 61.80%, H 3.79%, N 9.86%.

2-amino-4-(3-methoxyphenyl)-8-oxo-6-(trifluoromethyl)-4,8-dihydropyrano[3,2-*g*]chromene-3-carbonitrile (4f)

Yield: 89%; Pale yellow crystalline solid; MP: 214-216 °C; IR (KBr) ν: 3364 (NH_2), 2223 (CN), 1721 (C=C-C=O), 1622 (C=C), 1598, 1514, 1465, 1261 (Ar-OCH_3), 1217, 1169 (CF_3), 1127, 1086 cm^{-1}; ^{1}H-NMR (400 MHz, DMSO-d_6, TMS) δ: 3.77 (s, 3H, OCH_3), 4.65 (s, 1H, pyran-H), 6.37 (s, 1H, H-C=C), 6.82-6.88 (m, 2H, Ar-H), 7.08 (s, 2H, NH_2), 7.12 (s, 1H, Ar-H), 7.20-7.28 (m, 2H, Ar-H), 7.67 (s, 1H, Ar-H) ppm; ^{13}C-NMR (100 MHz, DMSO-d_6, TMS) δ: 36.2 (CH), 55.3 (OCH_3), 58.5 (C–CN), 112.1 (C–NH_2), 113.4 (Ar-C), 115.0 (Ar-C), 116.4 (Ar-C), 118.8 (C≡N), 122.4 (CF_3), 124.5 (Ar-C), 119.6 (Ar-C), 121.8 (Ar-C), 129.7 (Ar-C), 131.1 (Ar-C), 132.8 (Ar-C), 151.5 (Ar-C), 153.3 (Ar-C), 158.8 (Ar-C), 159.6 (Ar-C), 160.8 (Ar-C), 176.7 (C=O) ppm; ^{19}F-NMR (376 MHz, DMSO-d_6) δ: -62.421 (s, 3F, CF_3) ppm; ESI-MS m/z for ($C_{21}H_{13}F_3N_2O_4$) (414.08): 415.2 $(M+1)^+$; Elemental Analysis: Calculated for $C_{21}H_{13}F_3N_2O_4$ (414.33): C 60.88%, H 3.16%, N 6.76%; Found: C 60.85%, H 3.18%, N 6.79%.

2-amino-4-(4-chlorophenyl)-8-oxo-6-(trifluoromethyl)-4,8-dihydropyrano[3,2-*g*]chromene-3-carbonitrile (4g)

Yield: 92%; Yellow crystalline solid; MP: 228-230 °C; IR (KBr) ν: 3365 (NH_2), 2225 (CN), 1723 (C=C-C=O), 1624 (C=C), 1516, 1470, 1263, 1219, 1168 (CF_3), 1126, 1090, 821 (C–Cl) cm^{-1}; ^{1}H-NMR (400 MHz, DMSO-d_6, TMS) δ: 4.78 (s, 1H, pyran-H), 6.40 (s, 1H, Ar-H), 6.74 (s, 1H, coumarin-H), 7.08 (s, 2H, NH_2), 7.43 (d, *J* = 7.72 Hz, 2H, Ar-H), 7.78 (s, 1H, Ar-H), 8.12 (d, *J* = 9.48 Hz, 2H, Ar-H) ppm; ^{13}C-NMR (100 MHz, DMSO-d_6, TMS) δ: 36.2 (CH), 58.8 (C–CN), 112.4 (C–NH_2), 115.2 (Ar-C), 116.5 (Ar-C), 118.9 (C≡N), 122.5 (CF_3), 124.7 (Ar-C), 128.5 (Ar-C), 129.2 (Ar-C), 130.4 (Ar-C), 131.4 (Ar-C), 137.8 (Ar-C), 151.7 (Ar-C), 153.5 (Ar-C), 158.9 (Ar-C), 161.0 (Ar-C), 176.9 (C=O) ppm; ^{19}F-NMR (376 MHz, DMSO-d_6) δ: -62.420 (s, 3F, CF_3) ppm; ESI-MS m/z for ($C_{20}H_{10}ClF_3N_2O_3$) (418.03): 418.18 $(M)^+$, 420.13 $(M+2)^+$; Elemental Analysis: Calculated for $C_{20}H_{10}ClF_3N_2O_3$ (418.75): C 57.36%, H 2.41%, N 6.69%; Found: C 57.33%, H 2.43%, N 6.72%.

2-amino-4-(2-chlorophenyl)-8-oxo-6-(trifluoromethyl)-4,8-dihydropyrano[3,2-*g*]chromene-3-carbonitrile (4h)

Yield: 89%; Yellow crystalline solid; MP: 221-223 °C; IR (KBr) ν: 3364 (NH_2), 2224 (CN), 1722 (C=C-C=O), 1623 (C=C), 1515, 1468, 1262, 1218, 1168 (CF_3), 1125, 1088, 756 (C-Cl) cm^{-1}; ^{1}H-NMR (400 MHz, DMSO-d_6, TMS) δ: 4.65 (s, 1H, pyran-H), 6.40 (s, 1H, H-C=C), 7.11 (s, 2H, NH_2), 7.16-7.22 (m, 2H, Ar-H), 7.30-7.40 (m, 2H, Ar-H), 7.22 (s, 1H, Ar-H), 7.73 (s, 1H, Ar-H), 8.67 (s, 2H, NH_2) ppm; ^{13}C-NMR (100 MHz, DMSO-d_6, TMS) δ: 35.0 (CH), 58.6 (C–CN), 112.3 (C–NH_2), 115.1 (Ar-C), 116.4 (Ar-C), 118.8 (C≡N), 122.4 (CF_3), 124.6 (Ar-C), 127.4 (Ar-C), 128.1 (Ar-C), 129.5 (Ar-C), 130.8 (Ar-C), 131.3 (Ar-C), 134.9 (Ar-C), 136.6 (Ar-C), 151.6 (Ar-C), 153.4 (Ar-C), 158.8 (Ar-C), 160.9 (Ar-C), 176.8 (C=O) ppm; ^{19}F-NMR (376 MHz, DMSO-d_6) δ: -62.206 (s, 3F, CF_3) ppm; ESI-MS m/z for ($C_{20}H_{10}ClF_3N_2O_3$) (418.03): 418.1 $(M)^+$, 420.2 $(M+2)^+$; Elemental Analysis: Calculated for $C_{20}H_{10}ClF_3N_2O_3$ (418.75): C 57.36%, H 2.41%, N 6.69%; Found: C 57.39%, H 2.38%, N 6.71%.

2-amino-4-(4-bromophenyl)-8-oxo-6-(trifluoromethyl)-4,8-dihydropyrano[3,2-*g*]chromene-3-carbonitrile (4i)

Yield: 93%; Yellow crystalline solid; MP: 236-238 °C; IR (KBr) ν: 3365 (NH_2), 2225 (CN), 1723 (C=C-C=O), 1624 (C=C), 1516, 1469, 1263, 1219, 1168 (CF_3), 1127, 1089, 624 (C-Br) cm^{-1}; ^{1}H-NMR (400 MHz, DMSO-d_6, TMS) δ: 4.69 (s, 1H, pyran-H), 6.39 (s, 1H, H-C=C), 7.12 (s, 2H, NH_2), 7.21 (s, 1H, Ar-H), 7.40 (d, *J* = 8.4 Hz, 2H, Ar-H), 7.56 (d, *J* = 8.4 Hz, 2H, Ar-H), 7.72 (s, 1H, Ar-H) ppm; ^{13}C-NMR (100 MHz, DMSO-d_6, TMS) δ: 36.2 (CH), 58.8 (C–CN), 112.4 (C–NH_2), 115.2 (Ar-C), 116.5 (Ar-C), 118.9 (C≡N), 121.8 (Ar-C), 122.5 (CF_3), 124.7 (Ar-C), 129.0 (Ar-C), 130.7 (Ar-C), 131.4 (Ar-C), 138.2 (Ar-C), 151.7 (Ar-C), 153.5 (Ar-C), 158.9 (Ar-C), 161.0 (Ar-C), 176.9 (C=O) ppm; ^{19}F-NMR (376 MHz, DMSO-d_6) δ: -62.245 (s, 3F, CF_3) ppm; ESI-MS m/z for ($C_{20}H_{10}BrF_3N_2O_3$) (461.98): 462.0 $(M)^+$, 464.1 $(M+2)^+$; Elemental Analysis: Calculated for $C_{20}H_{10}BrF_3N_2O_3$ (463.21): C 51.86%, H 2.18%, N 6.05%; Found: C 51.83%, H 2.20%, N 6.08%.

2-amino-4-(2,5-dimethoxyphenyl)-8-oxo-6-(trifluoromethyl)-4,8-dihydropyrano[3,2-*g*]chromene-3-carbonitrile (4j)

Yield: 90%; Pale yellow crystalline solid; MP: 222-224 °C; IR (KBr) ν: 3364 (NH_2), 2222 (CN), 1720 (C=C-C=O), 1621 (C=C), 1596, 1513, 1464, 1264 (Ar-OCH_3), 1216, 1170 (CF_3), 1128, 1085 cm^{-1}; ^{1}H-NMR (400 MHz, DMSO-d_6, TMS) δ: 3.72 (s, 3H, OCH_3), 3.78 (s, 3H, OCH_3), 4.66 (s, 1H, pyran-H), 6.36 (s, 1H, H-C=C), 6.78 (d, *J* = 8.6 Hz, 1H, Ar-H), 6.92 (dd, *J* = 8.6, 2.8 Hz, 1H, Ar-H), 7.00 (s, 2H, NH_2), 7.05 (d, *J* = 2.8 Hz, 1H, Ar-H), 7.17 (s, 1H, Ar-H), 7.66 (s, 1H, Ar-H), 8.59 (s, 2H, NH_2) ppm; ^{13}C-NMR (100 MHz, DMSO-d_6, TMS) δ: 36.0 (CH), 55.5 (OCH_3), 56.1 (OCH_3), 58.4 (C–CN), 112.0 (C–NH_2), 112.8 (Ar-C), 114.5 (Ar-C), 115.1 (Ar-C), 116.4 (Ar-C), 118.7 (C≡N), 122.5 (CF_3), 124.4 (Ar-C), 116.8

(Ar-C), 120.3 (Ar-C), 130.8 (Ar-C), 151.4 (Ar-C), 152.8 (Ar-C), 153.2 (Ar-C), 154.6 (Ar-C), 158.7 (Ar-C), 160.8 (Ar-C), 176.7 (C=O) ppm; ^{19}F-NMR (376 MHz, DMSO-d$_6$) δ: -62.424 (s, 3F, CF$_3$) ppm; ESI-MS m/z for ($C_{22}H_{15}F_3N_2O_5$) (444.09): 445.2 $(M+1)^+$; Elemental Analysis: Calculated for $C_{22}H_{15}F_3N_2O_5$ (444.37): C 59.46%, H 3.40%, N 6.30%; Found: C 59.43%, H 3.42%, N 6.33%.

2-amino-8-oxo-6-(trifluoromethyl)-4-(3,4,5-trimethoxyphenyl)-4,8-dihydropyrano[3,2-*g*]chromene-3-carbonitrile (4k)

Yield: 92%; Pale yellow crystalline solid; MP: 226-228 °C; IR (KBr) ν: 3365 (NH$_2$), 2222 (CN), 1720 (C=C-C=O), 1621 (C=C), 1595, 1512, 1463, 1265 (Ar-OCH$_3$), 1217, 1169 (CF$_3$), 1128, 1084 cm^{-1}; ^{1}H-NMR (400 MHz, DMSO-d$_6$, TMS) δ: 3.63 (s, 3H, OCH$_3$), 3.73 (s, 6H, 2 × OCH$_3$), 4.66 (s, 1H, pyran-H), 6.42-6.58 (m, 4H, Ar-H and coumarin-H), 6.91 (s, 2H, NH$_2$) ppm, 7.74 (s, 1H, Ar-H); ^{13}C-NMR (100 MHz, DMSO-d$_6$, TMS) δ: 36.1 (CH), 56.0 (2 × OCH$_3$), 60.5 (OCH$_3$), 58.5 (C–CN), 104.8 (Ar-C), 112.1 (C–NH$_2$), 115.0 (Ar-C), 116.4 (Ar-C), 118.7 (C≡N), 122.5 (CF$_3$), 124.4 (Ar-C), 130.6 (Ar-C), 136.5 (Ar-C), 151.4 (Ar-C), 153.1 (Ar-C), 153.4 (Ar-C), 158.7 (Ar-C), 160.8 (Ar-C), 176.7 (C=O) ppm; ^{19}F-NMR (376 MHz, DMSO-d$_6$) δ: -62.399 (s, 3F, CF$_3$) ppm; ESI-MS m/z for ($C_{23}H_{17}F_3N_2O_6$) (474.10): 475.21 $(M+1)^+$; Elemental Analysis: Calculated for $C_{23}H_{17}F_3N_2O_6$ (474.39): C 58.23%, H 3.61%, N 5.91%; Found: C 58.20%, H 3.63%, N 5.94%.

2-amino-4-(4-fluorophenyl)-8-oxo-6-(trifluoromethyl)-4,8-dihydropyrano[3,2-*g*]chromene-3-carbonitrile (4l)

Yield: 91%; Yellow crystalline solid; MP: 223-225 °C; IR (KBr) ν: 3364 (NH$_2$), 2224 (CN), 1722 (C=C-C=O), 1623 (C=C), 1515, 1468, 1262, 1218, 1169 (CF$_3$), 1126, 1091, 1032 (C-F) cm^{-1}; ^{1}H-NMR (400 MHz, DMSO-d$_6$, TMS) δ: 4.67 (s, 1H, pyran-H), 6.38 (s, 1H, H-C=C), 7.05 (s, 2H, NH$_2$), 7.12-7.18 (m, 2H, Ar-H), 7.20 (s, 1H, Ar-H), 7.34-7.40 (m, 2H, Ar-H), 7.69 (s, 1H, Ar-H) ppm; ^{13}C-NMR (100 MHz, DMSO-d$_6$, TMS) δ: 36.3 (CH), 58.7 (C–CN), 112.3 (C–NH$_2$), 115.1 (Ar-C), 115.8 (d, J_CF = 21 Hz, Ar-C), 116.4 (Ar-C), 118.8 (C≡N), 122.4 (CF$_3$), 124.6 (Ar-C), 129.7 (Ar-C), 131.2 (Ar-C), 135.8 (Ar-C), 151.6 (Ar-C), 153.4 (Ar-C), 158.8 (Ar-C), 160.9 (Ar-C), 162.4 (d, J_CF = 246 Hz, Ar-C–F), 176.8 (C=O) ppm; ^{19}F-NMR (376 MHz, DMSO-d$_6$) δ: -62.328 (s, 3F, CF$_3$), -114.6 (m, 1F, Ar-F) ppm; ESI-MS m/z for ($C_{20}H_{10}F_4N_2O_3$) (402.06): 403.1 $(M+1)^+$; Elemental Analysis: Calculated for $C_{20}H_{10}F_4N_2O_3$ (402.30): C 59.71%, H 2.50%, N 6.96%; Found: C 59.68%, H 2.53%, N 6.99%.

2-amino-4-(4-nitrophenyl)-8-oxo-6-(trifluoromethyl)-4,8-dihydropyrano[3,2-*g*]chromene-3-carbonitrile (4m)

Yield: 88%; Bright yellow crystalline solid; MP: 242-244 °C; IR (KBr) ν: 3366 (NH$_2$), 2225 (CN), 1724 (C=C-C=O), 1625 (C=C), 1524 (NO$_2$ asym), 1348 (NO$_2$ sym), 1469, 1263, 1219, 1168 (CF$_3$), 1127, 1089 cm^{-1}; ^{1}H-NMR (400 MHz, DMSO-d$_6$, TMS) δ: 4.76 (s, 1H, pyran-H), 6.44 (s, 1H, Ar-H), 6.74 (s, 1H, coumarin-H), 7.04 (s, 2H, NH$_2$), 7.39 (d, *J* = 8.12 Hz, 2H, Ar-H), 7.78 (s, 1H, Ar-H), 8.12 (d, *J* = 10.28 Hz, 2H, Ar-H) ppm; ^{13}C-NMR (100 MHz, DMSO-d$_6$, TMS) δ: 36.5 (CH), 58.9 (C–CN), 112.5 (C–NH$_2$), 115.3 (Ar-C), 116.6 (Ar-C), 118.9 (C≡N), 122.5 (CF$_3$), 124.8 (Ar-C), 124.9 (Ar-C), 129.4 (Ar-C), 131.5 (Ar-C), 146.2 (Ar-C), 147.8 (Ar-C), 151.8 (Ar-C), 153.6 (Ar-C), 159.0 (Ar-C), 161.1 (Ar-C), 177.0 (C=O) ppm; ^{19}F-NMR (376 MHz, DMSO-d$_6$) δ: -62.429 (s, 3F, CF$_3$) ppm; ESI-MS m/z for ($C_{20}H_{10}F_3N_3O_5$) (429.06): 430.1 $(M+1)^+$; Elemental Analysis: Calculated for $C_{20}H_{10}F_3N_3O_5$ (429.31): C 55.95%, H 2.35%, N 9.79%; Found: C 55.92%, H 2.37%, N 9.82%.

2-amino-8-oxo-4-(pyridin-3-yl)-6-(trifluoromethyl)-4,8-dihydropyrano[3,2-*g*]chromene-3-carbonitrile (4n)

Yield: 87%; Yellow crystalline solid; MP: 231-233 °C; IR (KBr) ν: 3365 (NH$_2$), 2224 (CN), 1723 (C=C-C=O), 1624 (C=C), 1588 (C=N), 1516, 1467, 1262, 1218, 1169 (CF$_3$), 1126, 1088 cm^{-1}; ^{1}H-NMR (400 MHz, DMSO-d$_6$, TMS) δ: 4.60 (s, 1H, pyran-H), 6.40 (s, 1H, H-C=C), 7.09 (s, 2H, NH$_2$), 7.23 (s, 1H, Ar-H), 7.42 (dd, *J* = 8.0, 4.8 Hz, 1H, Py-H), 7.86 (d, *J* = 8.0 Hz, 1H, Py-H), 8.42 (d, *J* = 4.8 Hz, 1H, Py-H), 8.68 (s, 1H, Py-H), 8.73 (s, 1H, Ar-H); ^{13}C-NMR (100 MHz, DMSO-d$_6$, TMS) δ: 36.4 (CH), 58.8 (C-CN), 112.4 (C-NH$_2$), 115.2 (Ar-C), 116.5 (Ar-C), 118.9 (C≡N), 122.5 (CF$_3$), 123.8 (Py-C), 124.7 (Ar-C), 131.3 (Ar-C), 134.6 (Py-C), 136.2 (Py-C), 147.5 (Py-C), 149.2 (Py-C), 151.7 (Ar-C), 153.5 (Ar-C), 158.9 (Ar-C), 161.0 (Ar-C), 176.9 (C=O) ppm; ^{19}F-NMR (376 MHz, DMSO-d$_6$) δ: -62.249 (s, 3F, CF$_3$) ppm; ESI-MS m/z for ($C_{19}H_{10}F_3N_3O_3$) (385.07): 386.1 $(M+1)^+$; Elemental Analysis: Calculated for $C_{19}H_{10}F_3N_3O_3$ (385.30): C 59.23%, H 2.62%, N 10.91%; Found: C 59.20%, H 2.64%, N 10.94%.

2-amino-4-(furan-2-yl)-8-oxo-6-(trifluoromethyl)-4,8-dihydropyrano[3,2-*g*]chromene-3-carbonitrile (4o)

Yield: 86%; Light yellow crystalline solid; MP: 205-207 °C; IR (KBr) ν: 3364 (NH$_2$), 2223 (CN), 1721 (C=C-C=O), 1622 (C=C), 1568, 1514, 1465, 1261, 1217, 1169 (CF$_3$), 1127, 1086 cm^{-1}; ^{1}H-NMR (400 MHz, DMSO-d$_6$, TMS) δ: 4.68 (s, 1H, pyran-H), 6.28 (dd, *J* = 3.2, 1.8 Hz, 1H, furan-H), 6.37 (s, 1H, H-C=C), 6.54 (d, *J* = 3.2 Hz, 1H, furan-H), 7.08 (s, 2H, NH$_2$), 7.17 (s, 1H, Ar-H), 7.34 (d, *J* = 1.8 Hz, 1H, furan-H), 7.66 (s, 1H, Ar-H) ppm; ^{13}C-NMR (100 MHz, DMSO-d$_6$, TMS) δ: 31.8 (CH), 58.2 (C–CN), 108.6 (Fur-C), 110.9 (Fur-C), 112.2 (C–NH$_2$), 115.0 (Ar-C), 116.4 (Ar-C), 118.8 (C≡N), 122.4 (CF$_3$), 124.5 (Ar-C), 131.1 (Ar-C), 142.8 (Fur-C), 149.6 (Fur-C), 151.5 (Ar-C), 153.3 (Ar-C), 158.8 (Ar-C), 160.8 (Ar-C), 176.7 (C=O) ppm; ^{19}F-NMR (376 MHz, DMSO-d$_6$) δ: -62.409 (s, 3F, CF$_3$) ppm; ESI-MS m/z for ($C_{18}H_9F_3N_2O_4$) (374.05): 375.1 $(M+1)^+$; Elemental Analysis: Calculated for $C_{18}H_9F_3N_2O_4$ (374.27): C 57.76%, H 2.42%, N 7.48%; Found: C 57.73%, H 2.44%, N 7.51%.

2-amino-8-oxo-4-(thiophen-2-yl)-6-(trifluoromethyl)-4,8-dihydropyrano[3,2-*g*]chromene-3-carbonitrile (4p)

Yield: 87%; Yellow crystalline solid; MP: 218-220 °C; IR (KBr) ν: 3365 (NH_2), 2224 (CN), 1722 (C=C-C=O), 1623 (C=C), 1515, 1467, 1262, 1218, 1169 (CF_3), 1126, 1087, 742 (C-S) cm^{-1}; ^{1}H-NMR (400 MHz, DMSO-d_6, TMS) δ: 4.62 (s, 1H, pyran-H), 6.38 (s, 1H, H-C=C), 6.98 (dd, *J* = 5.0, 3.6 Hz, 1H, thiophene-H), 7.03 (s, 2H, NH_2), 7.15 (s, 1H, Ar-H), 7.24 (d, *J* = 3.6 Hz, 1H, thiophene-H), 7.46 (d, *J* = 5.0 Hz, 1H, thiophene-H), 7.68 (s, 1H, Ar-H) ppm; ^{13}C-NMR (100 MHz, DMSO-d_6, TMS) δ: 33.5 (CH), 58.4 (C–CN), 112.2 (C–NH_2), 115.1 (Ar-C), 116.4 (Ar-C), 118.8 (C≡N), 122.4 (CF_3), 124.5 (Ar-C), 126.8 (Thienyl-C), 127.9 (Thienyl-C), 128.6 (Thienyl-C), 131.2 (Ar-C), 142.4 (Thienyl-C), 151.5 (Ar-C), 153.3 (Ar-C), 158.8 (Ar-C), 160.8 (Ar-C), 176.8 (C=O) ppm; ^{19}F-NMR (376 MHz, DMSO-d_6) δ: -62.322 (s, 3F, CF_3) ppm; ESI-MS m/z for ($C_{18}H_9F_3N_2O_3S$) (390.03): 391.1 $(M+1)^+$; Elemental Analysis: Calculated for $C_{18}H_9F_3N_2O_3S$ (390.34): C 55.39%, H 2.32%, N 7.18%; Found: C 55.36%, H 2.34%, N 7.21%.

2.4. Antibacterial and antifungal activity

The synthesized trifluoromethyl coumarin-based 4*H*-pyran derivatives **(4a-p)** were evaluated for their *in vitro* antibacterial and antifungal activities using the broth dilution method.[51-53] Mueller-Hinton broth (MHB) was employed as the growth medium for bacterial strains, whereas Sabouraud dextrose broth (SDB) was used for fungal strains. The microbial inoculum for each test organism was prepared from freshly grown cultures and standardized to approximately 1×10^6 colony-forming units (CFU mL^{-1}) by adjusting the turbidity to match the appropriate McFarland standard.

Stock solutions of the synthesized compounds were prepared in dimethyl sulfoxide (DMSO) at a concentration of 2000 μg mL^{-1} and subsequently diluted with the corresponding sterile culture medium to obtain the desired test concentrations. The final concentration of DMSO in the assay system was maintained below 1% (v/v). Control experiments confirmed that DMSO at this concentration exhibited no detectable inhibitory effect on bacterial or fungal growth. The antimicrobial screening was performed in two stages. During the primary screening, test compounds were evaluated at concentrations of 1000, 500, 250, and 125 μg mL^{-1}. Compounds demonstrating significant growth inhibition in the initial screening were subjected to secondary evaluation using lower concentrations of 100, 62.5, 50, 25, 12.5, and 6.25 μg mL^{-1}. Following inoculation, bacterial cultures were incubated at 37 °C for 24h, whereas fungal cultures were incubated at 28 ± 2 °C for 48-72 h. Growth controls containing only inoculated culture medium, sterility controls containing uninoculated medium, and solvent controls containing the corresponding concentration of DMSO were included in each experiment. The minimum inhibitory concentration (MIC) was defined as the lowest concentration of the test compound that inhibited at least 99% of visible microbial growth when compared with the untreated control. Prior to inoculation, a loopful of each microbial suspension was subcultured onto the corresponding agar medium to verify culture purity, viability, and suitability of the growth conditions.

All synthesized compounds **(4a-p)** were screened against two Gram-positive bacterial strains, *Staphylococcus aureus* (MTCC 96) and *Streptococcus pyogenes* (MTCC 442); two Gram-negative bacterial strains, *Escherichia coli* (MTCC 443) and *Pseudomonas aeruginosa* (MTCC 1688); and three fungal strains, *Candida albicans* (MTCC 227), *Aspergillus niger* (MTCC 282), and *Aspergillus clavatus* (MTCC 1323). Ampicillin, Ciprofloxacin, and Chloramphenicol were employed as reference antibacterial agents, whereas Nystatin and griseofulvin were used as standard antifungal drugs for comparison.

All antimicrobial assays were performed independently in triplicate (n = 3), and the results are expressed as mean. Statistical analysis was carried out using one-way analysis of variance (ANOVA) followed by Tukey's post hoc multiple comparison test. Differences were considered statistically significant at $p < 0.05$. The low standard deviation values obtained among replicate experiments confirmed the reliability and reproducibility of the antimicrobial assays.

3. Result and discussion

3.1 Chemistry and reaction optimization

Initially, the synthesis of 2-amino-8-oxo-4-phenyl-6-(trifluoromethyl)-4,8-dihydropyrano[3,2-*g*]chromene-3-carbonitrile **(4a)** was selected as a model reaction involving 7-hydroxy-4-(trifluoromethyl)coumarin, benzaldehyde, and malononitrile. To establish an efficient and environmentally benign synthetic protocol, various reaction parameters including catalyst type, catalyst loading, solvent system, and microwave power were systematically optimized.

The catalytic efficiency of several acidic catalysts was initially examined and the results are summarized in **Table 1**. In the absence of catalyst **(Table 1, entry 1)**, only trace product formation was observed even after 20 minutes of microwave irradiation, demonstrating the necessity of catalytic activation for the Knoevenagel-Michael cyclization sequence. Acetic acid and citric acid afforded moderate yields of 52% and 74%, respectively **(Table 1, entries 2-3)**, indicating that acidic activation promotes the reaction but is insufficient to achieve complete conversion within a short reaction time. A further improvement was observed using *p*-TSA, which furnished the desired product in 81% yield within 8 min **(Table 1, entry 4)**. Although concentrated sulfuric acid provided a high yield of 88% in only 6 min **(Table 1, entry 5)**, its corrosive nature and environmental concerns limit its practical utility. Tamarind juice, another naturally occurring acidic medium, afforded the desired product in 76% yield **(Table 1, entry 6)**. Among all catalysts investigated, freshly extracted lemon juice proved to be the most effective, furnishing compound **(4a)** in 89% yield within 6 min **(Table 1, entry 7)**. The superior catalytic activity of lemon juice can be attributed to the synergistic effect of naturally occurring citric acid, ascorbic acid, malic acid,

and other organic constituents, which collectively facilitate the Knoevenagel condensation, Michael addition, and subsequent cyclization steps. In addition to its excellent catalytic performance, lemon juice offers significant advantages such as biodegradability, renewability, low cost, easy availability, and compliance with green chemistry principles.

Table 1. Optimization of catalyst for the synthesis of compound **(4a)**[a]

Entry	Catalyst	Conditions	Time (min)	Yield (%)[b]
1	None	MWI, 300 W	20	Trace
2	Acetic acid	MWI, 300 W	15	52
3	Citric acid	MWI, 300 W	10	74
4	*p*-TSA	MWI, 300 W	8	81
5	Conc. H_2SO_4	MWI, 300 W	6	88
6	Tamarind juice	MWI, 300 W	10	76
7	**Lemon juice**	**MWI, 300 W**	**6**	**89**

[a]**Reaction conditions:** 7-hydroxy-4-(trifluoromethyl)coumarin (0.031 mol), benzaldehyde (0.031 mol), malononitrile (0.032 mol), ethanol:water (1:1), microwave irradiation (MWI).
[b] = isolated yield

Having identified lemon juice as the optimal catalyst, its loading was subsequently optimized **(Table 2)**. At lower catalyst loadings, incomplete conversion was observed, resulting in prolonged reaction times and diminished yields. The use of only 1 mL of lemon juice afforded the desired product in 48% yield after 15 min **(Table 2, entry 1)**. Increasing the catalyst loading to 2 and 3 mL significantly improved the yield to 63% and 76%, respectively, while simultaneously reducing the reaction time to 12 and 10 min **(Table 2, entries 2-3)**. A substantial enhancement was achieved when the catalyst loading was increased to 5 mL, affording compound **(4a)** in 89% yield within only 6 min **(Table 2, entry 4)**. Interestingly, further increases in catalyst loading to 7 and 10 mL did not provide any significant improvement in yield or reaction time **(Table 2, entries 5-6)**, indicating that the catalytic system had reached its optimum efficiency. Therefore, 5 mL of freshly extracted lemon juice was selected as the optimum catalyst loading for all subsequent studies.

Table 2. Optimization of lemon juice loading for the synthesis of compound **(4a)**[a]

Entry	Lemon juice (mL)	Time (min)	Yield (%)[b]
1	1.0	15	48
2	2.0	12	63
3	3.0	10	76
4	**5.0**	**6**	**89**
5	7.0	6	89
6	10.0	6	88

[a]**Reaction conditions:** 7-hydroxy-4-(trifluoromethyl)coumarin (0.031 mol), benzaldehyde (0.031 mol), malononitrile (0.032 mol), ethanol:water (1:1), microwave irradiation (MWI).
[b] = isolated yield

The influence of solvent on the model reaction was then investigated and the results are presented in **Table 3**. Solvent selection was found to have a pronounced effect on both reaction rate and isolated yield. When the reaction was performed in water, poor solubility of the reactants resulted in a relatively low yield of 51% after 15 min **(Table 3, entry 1)**. Ethanol and methanol afforded improved yields of 78% and 74%, respectively **(Table 3, entries 2-3)**, owing to their ability to dissolve the reaction components more effectively. Polar aprotic solvents such as acetonitrile and DMF provided only moderate yields **(Table 3, entries 4-5)**. Notably, the ethanol:water mixture (1:1) furnished the best result, affording compound **(4a)** in 89% yield within 6 min **(Table 3, entry 6)**. The superior performance of this hydroalcoholic medium may be attributed to enhanced substrate solubility, efficient catalyst dispersion, and favourable microwave absorption characteristics. Furthermore, the product readily precipitated from the reaction medium upon cooling, simplifying isolation and minimizing purification requirements. Additional experiments employing ethanol:water mixtures in ratios of 1:4 and 4:1 resulted in lower yields of 75% and 83%, respectively **(Table 3, entries 7-8)**, confirming that a 1:1 solvent composition provides the optimum balance between solubility and reaction efficiency.

Table 3. Solvent screening for the synthesis of compound **(4a)**[a]

Entry	Solvent	Time (min)	Yield (%)[b]
1	Water	15	51
2	Ethanol	10	78
3	Methanol	10	74
4	Acetonitrile	12	61
5	DMF	15	57
6	**Ethanol:Water (1:1)**	**6**	**89**
7	Ethanol:Water (1:4)	15	75
8	Ethanol:Water (4:1)	15	83

[a]**Reaction conditions:** 7-hydroxy-4-(trifluoromethyl)coumarin (0.031 mol), benzaldehyde (0.031 mol), malononitrile (0.032 mol), lemon juice (5 mL), microwave irradiation (MWI).
[b] = isolated yield

To further improve reaction efficiency and reduce energy consumption, microwave irradiation was employed and optimized **(Table 4)**. At a microwave power of 100 W, only 42% yield was obtained after 20 min **(Table 4, entry 1)**. Increasing the

power to 200 W improved the yield to 68% while reducing the reaction time to 12 min **(Table 4, entry 2)**. The best result was achieved at 300 W, where the desired product was obtained in 89% yield within only 6 min **(Table 4, entry 3)**. Further increases in microwave power to 400 and 500 W did not improve the outcome and resulted in slightly lower yields of 87% and 83%, respectively **(Table 4, entries 4-5)**, possibly due to localized overheating or minor side reactions. For comparison, the reaction was also performed under conventional reflux conditions, which required 240 min to furnish the product in only 76% yield **(Table 4, entry 6)**. These results clearly demonstrate the superiority of microwave-assisted synthesis, which dramatically reduced reaction time while simultaneously enhancing product yield through rapid and uniform volumetric heating.

Table 4. Optimization of microwave power for the synthesis of compound **(4a)**[a]

Entry	Conventional heating condition	Microwave power (W)	Time (min)	Yield (%)[b]
1	-	100	20	42
2	-	200	12	68
3	**-**	**300**	**6**	**89**
4	-	400	5	87
5	-	500	5	83
6	Reflux	-	240	76

[a]**Reaction conditions:** 7-hydroxy-4-(trifluoromethyl)coumarin (0.031 mol), benzaldehyde (0.031 mol), malononitrile (0.032 mol), lemon juice (5 mL), ethanol:water (1:1).
[b] = isolated yield

With the optimized reaction conditions in hand, namely lemon juice (5 mL) as catalyst, ethanol:water (1:1) as solvent, and microwave irradiation at 300 W, the substrate scope of the methodology was explored using a variety of aromatic and heteroaromatic aldehydes. The results are summarized in **Table 5**. Gratifyingly, all investigated aldehydes underwent smooth conversion to afford the corresponding trifluoromethyl coumarin-based pyrano[3,2-*g*]chromene derivatives **(4a-p)** in excellent yields (86-94%). Electron-withdrawing substituents generally promoted faster reactions, as evidenced by the nitro- and halogen-substituted aldehydes. For example, 4-nitrobenzaldehyde and 4-fluorobenzaldehyde furnished compounds **(4m)** and **(4l)** in 94% and 93% yields within 4-6 min, respectively **(Table 5, entries 12-13)**. Similarly, 4-bromobenzaldehyde and 4-chlorobenzaldehyde afforded compounds **(4i)** and **(4g)** in 94% and 92% yields within only 5 min **(Table 5, entries 7-9)**. This behaviour can be attributed to the increased electrophilicity of the aldehyde carbonyl group, facilitating the initial Knoevenagel condensation with malononitrile.

Table 5. Synthesis of trifluoromethyl coumarin-based 4*H*-pyran derivatives (**4a-p**) catalyzed by lemon juice along with Turnover Number (TON) and Turnover Frequency (TOF) calculation

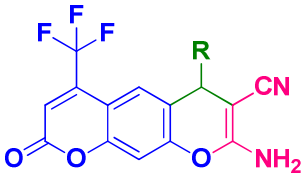

(4a-p)

Entry	Product Code	R	Time (min)	Yield (%)[a]	(Mp °C) Found	Product formed (mmol)	TON[b]	TOF (h^{-1})[c]
1	**(4a)**	C_6H_5	6	89	212-214	27.59	17.69	176.9
2	**(4b)**	4-OCH_3-C_6H_4	7	92	204-207	28.52	18.28	156.7
3	**(4c)**	4-CH_3-C_6H_4	7	88	198-200	27.28	17.49	149.9
4	**(4d)**	2-CH_3-C_6H_4	8	91	194-196	28.21	18.08	135.6
5	**(4e)**	4-$N(CH_3)_2$-C_6H_4	8	89	190-192	27.59	17.69	132.7
6	**(4f)**	3-OCH_3-C_6H_4	7	86	201-203	26.66	17.09	146.5
7	**(4g)**	4-Cl-C_6H_4	5	92	226-228	28.52	18.28	219.4
8	**(4h)**	2-Cl-C_6H_4	6	88	217-219	27.28	17.49	174.9
9	**(4i)**	4-Br-C_6H_4	5	94	232-234	29.14	18.68	224.2
10	**(4j)**	2,5-diOMe-C_6H_3	8	86	196-198	26.66	17.09	128.2
11	**(4k)**	3,4,5-triOMe-C_6H_2	8	88	190-192	27.28	17.49	131.2
12	**(4l)**	4-F-C_6H_4	6	93	238-240	28.83	19.22	230.6
13	**(4m)**	4-NO_2-C_6H_4	4	94	244-246	29.14	18.68	280.2
14	**(4n)**	3-Pyridyl	6	88	221-223	27.28	17.49	174.9
15	**(4o)**	2-Furyl	6	86	202-204	26.66	17.09	170.9
16	**(4p)**	2-Thienyl	6	87	208-210	26.97	17.29	172.9

Reaction conditions: 7-hydroxy-4-(trifluoromethyl)coumarin (0.031 mol), aldehyde (0.031 mol), malononitrile (0.032 mol), lemon juice (5 mL), ethanol:water (1:1), MWI, 300 W.
[a]Isolated yield of the pure product.
[b]Turnover number (average number of product molecules produced per mole of the catalyst).
[c]Turnover frequency (turnover number per time).

Aldehydes bearing electron-donating substituents such as methoxy, methyl, dimethylamino, and polymethoxy groups also reacted efficiently, affording the desired products in excellent yields ranging from 86-92% **(Table 5, entries 2-6 and 10-11)**. Although these substrates generally required slightly longer reaction times (7-9 min), the isolated yields remained comparable to those obtained with electron-withdrawing substituents. The *ortho*-substituted derivatives **(4d)** and **(4h)** required marginally longer reaction times than their *para*-substituted analogues, likely due to steric effects that hinder the approach of the reacting species during the condensation step. Furthermore, heteroaromatic aldehydes such as 3-pyridyl, 2-furyl, and 2-thienyl aldehydes participated smoothly in the reaction, affording compounds **(4n-p)** in 86-88% yields within 6 min **(Table 5, entries 14-16)**. These findings demonstrate the broad substrate scope, excellent functional-group tolerance, and practical applicability of the present lemon-juice-catalyzed microwave-assisted multicomponent protocol for the rapid synthesis of structurally diverse trifluoromethyl coumarin-based 4*H*-pyran hybrids. To obtain the pure target compounds, the crude mixture was simply recrystallized using ethanol. This protocol completely eliminates the need for column chromatography or alternative separation methods.

3.2. Catalyst recyclability and efficacy

To further assess the catalytic efficiency of the developed lemon-juice-catalyzed protocol, the turnover number (TON) and turnover frequency (TOF) were estimated for the model reaction leading to compound **(4a)**. Since lemon juice is a naturally occurring catalytic system composed primarily of citric acid along with malic acid, ascorbic acid, and other organic constituents, the catalytic activity was approximated based on the citric acid content present in freshly extracted lemon juice. Fresh lemon juice typically contains approximately 5-6 wt% citric acid. Accordingly, 5 mL of lemon juice (≈ 5 g) used under the optimized reaction conditions was estimated to contain about 0.30 g of citric acid, corresponding to 1.56 mmol of catalytically active acidic species. Under the optimized reaction conditions, the model reaction afforded compound **(4a)** in 89% isolated yield within 6 min **(Table 5, entry 1)**, corresponding to the formation of 27.59 mmol of product from 31 mmol of starting aldehyde. The turnover number (TON) and turnover frequency (TOF) were calculated according to **Equations (1) and (2):**

Equations (1): TON = (moles of product formed)/(moles of catalyst)

Equations (2): TOF = TON/(reaction time, h)

Substitution of the experimental values afforded a TON value of 17.69 and a TOF value of 176.9 h^{-1} for model reaction **(4a)**. Similarly, the turnover number (TON) and turnover frequency (TOF) values were calculated for the entire series of synthesized trifluoromethyl coumarin-based 4*H*-pyran derivatives **(Table 5)**. The obtained TON values ranged from 17.09 to 18.68, while the corresponding TOF values were found to be in the range of 128.2-280.2 h^{-1}. The relatively high TOF values observed under microwave irradiation clearly demonstrate the excellent catalytic efficiency of the lemon juice–microwave system. The enhanced catalytic performance can be attributed to the synergistic effect of rapid microwave-assisted dielectric heating and the naturally occurring organic acids present in lemon juice, which collectively accelerate the Knoevenagel condensation, Michael addition, and cyclization processes. These results further support the effectiveness of lemon juice as a sustainable, inexpensive, and environmentally benign bio-catalyst for the rapid synthesis of trifluoromethyl coumarin-based pyrano[3,2-*g*]chromene derivatives.

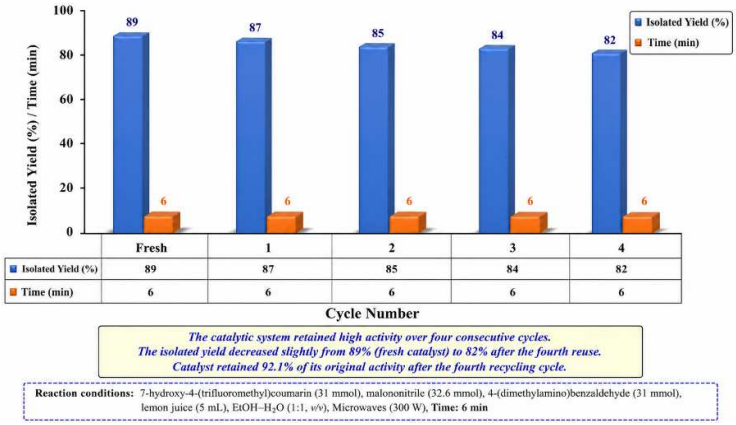

Fig. 2. Reusability study of the lemon juice catalyst for the synthesis of compound (**4a**) under optimized microwave-assisted conditions

The recyclability of the catalytic system was investigated using the model synthesis of compound **(4a)** under the optimized reaction conditions. After completion of the reaction, the solid product was removed by filtration and the catalyst-containing filtrate was directly reused for subsequent cycles after replenishing the reactants. As shown in **Fig. 5**, the catalytic system retained excellent activity over four consecutive cycles. The isolated yield decreased only slightly from 89% for the fresh catalyst to 87%, 85%, 84%, and 82% after the first, second, third, and fourth reuse cycles, respectively. The minor reduction in catalytic efficiency may be attributed to partial loss of acidic constituents during handling and repeated processing. Nevertheless, the results clearly demonstrate the operational stability, recyclability, and practical utility of lemon juice as a sustainable and environmentally benign catalyst for the microwave-assisted synthesis of trifluoromethyl coumarin-based 4*H*-pyran derivatives.

The catalyst recycling experiment **(Fig. 2)** revealed that the recovered lemon juice catalyst maintained high catalytic efficiency throughout four consecutive cycles. Only a marginal decrease in isolated yield was observed from 89% for the fresh catalyst to 82% after the fourth reuse, confirming the robustness and sustainability of the catalytic system. The catalyst retained 92.1% of its original activity after the fourth recycling cycle.

3.3. Spectroscopic characterization

The structures of all synthesized trifluoromethylated pyrano[3,2-*g*]chromene derivatives **(4a-p)** were unambiguously established using FT-IR, ^{1}H-NMR, ^{13}C-NMR, ^{19}F-NMR, EI-MS, and elemental analysis. The spectral data obtained for all compounds were in excellent agreement with the proposed molecular structures and confirmed the successful formation of the desired 2-amino-3-cyano-6-(trifluoromethyl)-4*H*-pyrano[3,2-*g*]chromene scaffold.

In the FT-IR spectra, all compounds exhibited characteristic absorption bands corresponding to the amino group at 3362-3366 cm^{-1} and the nitrile functionality at 2221-2225 cm^{-1}, confirming the presence of the 2-amino-3-cyano moiety. A strong absorption band observed between 1720 and 1724 cm^{-1} was attributed to the conjugated lactone carbonyl group of the chromene ring system. Additional absorptions around 1620-1625 cm^{-1} corresponded to C=C stretching vibrations within the fused heterocyclic framework. The trifluoromethyl substituent consistently displayed characteristic C-F stretching vibrations at 1168-1171 cm^{-1}. Furthermore, methoxy-substituted derivatives **(4b)**, **(4f)**, **(4j)**, and **(4k)** exhibited additional Ar-OCH_3 stretching bands near 1258-1265 cm^{-1}, whereas halo-substituted compounds displayed characteristic C-Cl, C-Br, and C-F absorptions in the fingerprint region.

The ^{1}H-NMR spectra showed a characteristic singlet for the newly formed pyran-H proton in the range δ 4.60-4.86 ppm, confirming the formation of the dihydropyrano ring system. The NH_2 protons generally appeared as singlets in the δ 6.91-7.12 ppm region, while the characteristic coumarin/olefinic proton was observed around δ 6.34-6.76 ppm. The remaining signals corresponded well with the aromatic and substituent protons of the respective derivatives. For example, the p-tolyl derivative 4c exhibited a methyl singlet at δ 2.28 ppm, whereas methoxy-substituted derivatives showed OCH_3 signals around δ 3.63-3.78 ppm.

The ^{13}C-NMR spectra further supported the proposed structures, with the pyran methine carbon appearing around δ 31.8-36.5 ppm and the C-CN carbon at δ 58.2-58.9 ppm. The nitrile carbon was consistently observed near δ 118.7-118.9 ppm, while the CF_3 carbon appeared around δ 122.4-122.5 ppm. The conjugated carbonyl carbon was consistently identified at approximately δ 176.6-177.0 ppm. Substituent-specific resonances, including OCH_3, CH_3, $N(CH_3)_2$ and heteroaryl carbons, were also consistent with the assigned structures.

The ^{19}F-NMR spectra of the synthesized compounds exhibited a characteristic singlet for the CF_3 group in the narrow range of δ -62.21 to -62.43 ppm, providing additional confirmation of the trifluoromethyl substituent. For the 4-fluorophenyl derivative 4l, an additional fluorine resonance was observed at δ -114.6 ppm, together with the expected ^{13}C-^{19}F coupling, confirming the presence of the aryl-F group.

The molecular structures were additionally verified by EI-mass spectrometry. Each compound displayed a molecular ion peak corresponding to the expected $(M+1)^+$ ion, which was in excellent agreement with the calculated exact mass values. For example, compound **(4a)** exhibited a molecular ion peak at m/z 385.1 $(M+1)^+$, consistent with its molecular formula $C_{20}H_{11}F_3N_2O_3$. Substituted derivatives showed the anticipated increases in molecular mass according to the nature of the aryl or heteroaryl substituent. Importantly, the halogen-containing derivatives provided additional diagnostic evidence through their isotopic patterns. The chloro-substituted compounds **(4g)** and **(4h)** exhibited characteristic M and M+2 isotope peaks in an approximate 3:1 intensity ratio, confirming the presence of a single chlorine atom. Likewise, the bromo-substituted derivative **(4i)** displayed a distinctive M and M+2 isotope pattern of nearly equal intensity (1:1 ratio), which is characteristic of a single bromine atom. These isotopic signatures provided strong support for the successful incorporation of the respective halogen substituents into the pyranochromene framework.

Finally, elemental analysis data for all compounds showed excellent agreement between calculated and experimentally found percentages of carbon, hydrogen, and nitrogen, with deviations falling within acceptable analytical limits. The close

correspondence between theoretical and experimental values further confirmed the high purity and structural integrity of the synthesized compounds. Overall, the combined FT-IR, ^{1}H-NMR, ^{13}C-NMR, ^{19}F-NMR, EI-MS, and elemental analytical data conclusively established the structures of the synthesized trifluoromethylated pyrano[3,2-*g*]chromene derivatives **(4a-p)**, thereby validating the efficiency of the lemon juice-catalyzed multicomponent synthetic methodology.

3.4. Kinetic study of the model reaction

To gain insight into the reaction pathway and catalytic efficiency of lemon juice, a kinetic investigation was performed using the model reaction leading to compound (**4e**). The reaction mixture consisting of 7-hydroxy-4-(trifluoromethyl)coumarin (31 mmol), malononitrile (32.6 mmol), and 4-(dimethylamino)benzaldehyde (31 mmol) in 100 mL of ethanol:water (1:1, v/v) containing freshly extracted lemon juice (5 mL) was subjected to microwave irradiation at 300 W. Aliquots (0.50 mL) were withdrawn at regular intervals of 1 min during the course of the reaction and immediately cooled in an ice bath to quench further conversion. Each aliquot was extracted with ethyl acetate (2.5 mL), suitably diluted, and analyzed using a UV-visible spectrophotometer in a quartz cuvette with a 1 cm path length. Now, this solution was diluted with ethyl acetate to make it 16 nM. UV-visible spectra were recorded at every 1 minute interval in the range of 250-600 nm for at least 6 minutes at 25 ºC of above diluted solution **(Fig. 3)**.

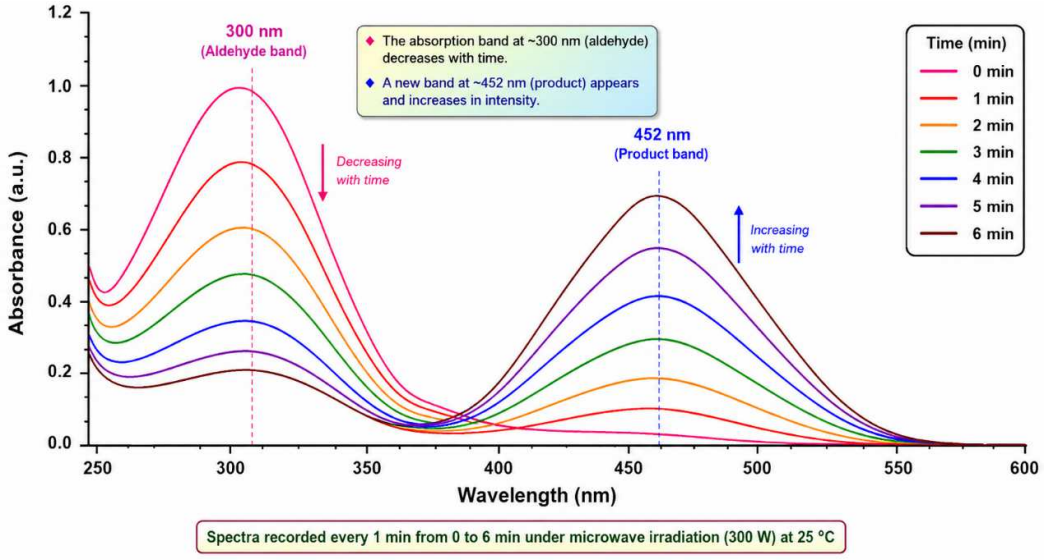

¶ **Fig. 3.** UV-visible spectra recorded during the formation of compound **(4e)** under microwave irradiation (300 W) at 1 min intervals

The starting aldehyde exhibited a characteristic absorption band at approximately 300 nm, which progressively decreased during microwave irradiation. Simultaneously, a new absorption band centered at approximately 452 nm appeared and increased in intensity, corresponding to the formation of the desired pyrano[3,2-*g*]chromene derivative **(Fig. 3)**. The reaction progress was monitored by measuring the absorbance at 300 nm corresponding to the aldehyde substrate. The experimental absorbance values recorded at different time intervals are summarized in **Table 6**.

Table 6. Kinetic data for the formation of compound **(4e)** monitored at 300 nm under microwave irradiation (300 W)

Time (min)	Absorbance (At)	At/A0	ln(At/A0)
0	1.000	1.000	0.000
1	0.780	0.780	-0.248
2	0.610	0.610	-0.494
3	0.470	0.470	-0.755
4	0.360	0.360	-1.022
5	0.280	0.280	-1.273
6	0.210	0.210	-1.561

A continuous decrease in absorbance at 300 nm was observed as reaction time increased, indicating rapid consumption of the aldehyde substrate under the optimized reaction conditions. The corresponding plot of absorbance versus time **(Fig. 4)** revealed a sharp decline during the first few minutes of microwave irradiation, confirming the accelerated nature of the transformation.

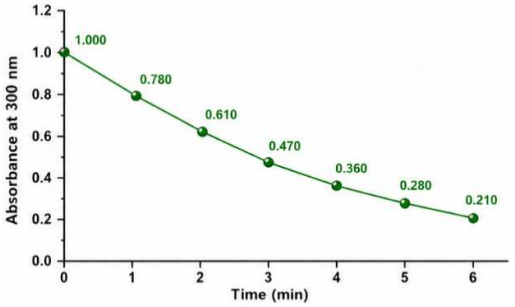

Fig. 4. Plot of absorbance at 300 nm versus reaction time for the synthesis of compound **(4e)** under microwave-assisted conditions

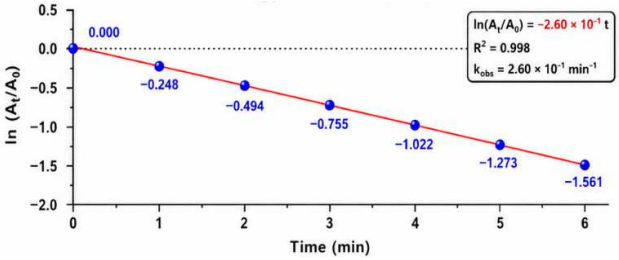

Fig. 5. Plot of ln(At/A0) versus reaction time for the formation of compound **(4e)** showing pseudo-first-order kinetic behaviour

To determine the reaction order, a plot of ln(At/A0) versus time was constructed **(Fig. 5)**. The excellent linear relationship (R^2 = 0.998) indicates that the reaction exhibited apparent pseudo-first-order kinetics with respect to the aldehyde concentration under the employed experimental conditions. The rate constant was calculated using the first-order kinetic equation:

ln(At/A0) = -kt

where A0 and At represent the absorbance values at time zero and time t, respectively.

From the slope of the linear plot, the apparent pseudo-first-order rate constant was determined to be **2.60×10^{-1} min^{-1}**. The relatively high-rate constant clearly demonstrates the remarkable catalytic efficiency of the lemon juice-microwave system. The apparent rate constant ($k_{obs} = 2.60 \times 10^{-1}$ min^{-1}) corresponds to a half-life ($t_{1/2} = \ln 2/k$) of approximately 2.67 min, which is consistent with the rapid product formation observed experimentally under microwave irradiation. It should be noted that the obtained pseudo-first-order kinetic parameters describe the apparent overall reaction behavior under the employed experimental conditions and do not represent the rate constant of any individual elementary step within the consecutive Knoevenagel condensation, Michael addition, and cyclization sequence. The observed rate enhancement may be attributed to the combined effect of rapid dielectric heating under microwave irradiation and the catalytic action of naturally occurring organic acids present in lemon juice, including citric acid, malic acid, and ascorbic acid. These acidic constituents facilitate aldehyde activation and promote the sequential Knoevenagel condensation, Michael addition, and intramolecular cyclization steps leading to product formation.

The kinetic results are in excellent agreement with the optimization studies presented in **Tables 1-4** and the substrate scope study shown in **Table 5**, where the desired trifluoromethyl coumarin-based 4*H*-pyran derivatives were obtained within 4-8 min in excellent isolated yields (86-94%). The rapid substrate consumption observed during the kinetic investigation further validates the efficiency of the developed microwave-assisted lemon-juice-catalyzed protocol and highlights its potential as a sustainable and environmentally benign approach for the synthesis of biologically important pyranochromene hybrids.

3.5. Antimicrobial activity

3.5.1. In vitro antibacterial activity

The synthesized trifluoromethyl coumarin-based 4*H*-pyran derivatives **(4a-p)** were evaluated for their antibacterial activity against two Gram-negative bacterial strains (*Escherichia coli* MTCC 443 and *Pseudomonas aeruginosa* MTCC 1688) and two Gram-positive bacterial strains (*Staphylococcus aureus* MTCC 96 and *Streptococcus pyogenes* MTCC 442). The minimum inhibitory concentration (MIC) values are summarized in **Table 6**. MIC values reported in **Table 6** represent the modal MIC obtained from three independent experiments. Replicate assays produced identical or highly consistent MIC values, indicating good reproducibility of the antibacterial evaluation. Ampicillin, Ciprofloxacin, and Chloramphenicol were used as reference antibacterial drugs for comparison. Overall, the synthesized compounds exhibited moderate to excellent antibacterial activity, with MIC values ranging from 25 to 250 µg/mL **(Fig. 6)**. A pronounced dependence of antibacterial potency on the nature and position of the substituent attached to the aryl ring was observed, indicating a clear structure-activity relationship.

Table 6. *In vitro* antibacterial activity[a] of trifluoromethyl coumarin-based 4*H*-pyran derivatives **(4a-p)**

Compound Code	R	MIC [µg/mL]			
		E. Coli MTCC 443	*P. Aeruginosa* MTCC 1688	*S. Aureus* MTCC 96	*S. Pyogenus* MTCC 442
(4a)	C_6H_5	125	125	100	100
(4b)	4-OCH_3-C_6H_4	200	250	125	125
(4c)	4-CH_3-C_6H_4	200	200	125	125
(4d)	2-CH_3-C_6H_4	250	250	125	125
(4e)	4-$N(CH_3)_2$-C_6H_4	250	250	200	200
(4f)	3-OCH_3-C_6H_4	200	200	125	125
(4g)	4-Cl-C_6H_4	62.5	62.5	50	50
(4h)	2-Cl-C_6H_4	100	100	62.5	62.5
(4i)	4-Br-C_6H_4	50	62.5	25	25
(4j)	2,5-diOMe-C_6H_3	200	250	125	125
(4k)	3,4,5-triOMe-C_6H_2	250	250	125	125
(4l)	4-F-C_6H_4	25	50	25	25
(4m)	4-NO_2-C_6H_4	25	62.5	25	25
(4n)	3-Pyridyl	62.5	62.5	50	50
(4o)	2-Furyl	100	100	62.5	62.5
(4p)	2-Thienyl	62.5	62.5	50	50
Ampicillin		100	100	250	100
Ciprofloxacin		25	25	50	50
Chloramphenicol		50	50	50	50

[a] = Values represent the mean of three independent experiments (n = 3). DMSO (≤1%, v/v) showed no inhibitory effect on microbial growth. Statistical significance was evaluated by one-way ANOVA followed by Tukey's multiple comparison tests ($p < 0.05$).

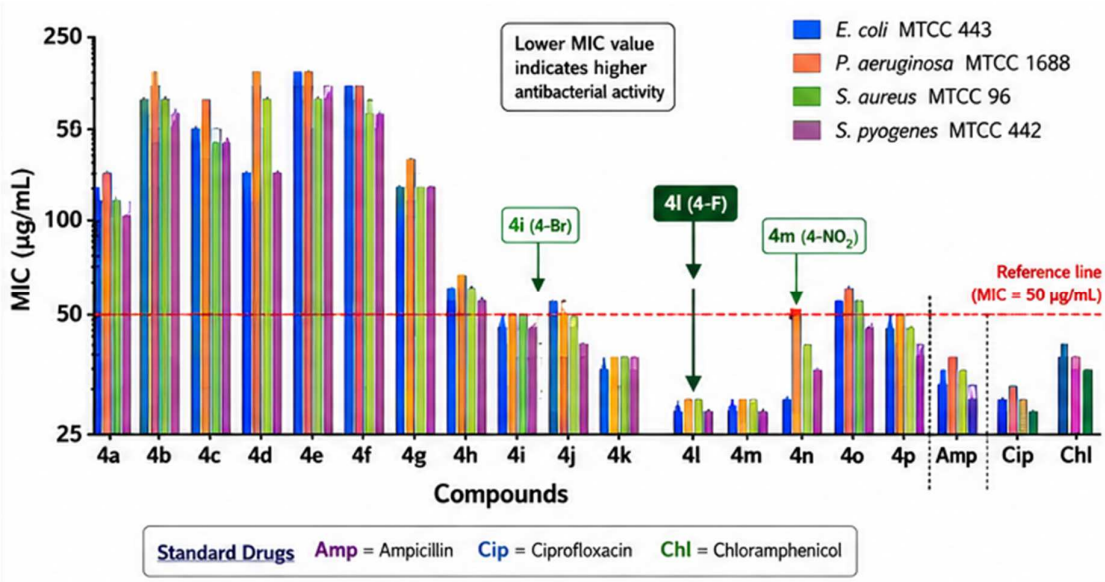

Fig. 6. Antibacterial activity of trifluoromethyl coumarin-based 4*H*-pyran derivatives **(4a-p)**

Among the entire series, compounds bearing electron-withdrawing substituents demonstrated the highest antibacterial activity. The *para*-fluoro derivative **(4l)** emerged as one of the most potent compounds, exhibiting MIC values of 25 µg/mL against *E. coli* and both Gram-positive strains (*S. aureus* and *S. pyogenes*). Likewise, the *para*-nitro analogue **(4m)** showed remarkable antibacterial potency, displaying MIC values of 25 µg/mL against *E. coli*, *S. aureus*, and *S. pyogenes*. These activities are comparable to those of the reference antibiotic Ciprofloxacin and superior to Ampicillin and Chloramphenicol against several tested strains. The enhanced activity of compounds **(4l)** and **(4m)** may be attributed to the strong electron-

withdrawing nature of fluorine and nitro groups, which increases molecular polarity, improves membrane penetration, and promotes stronger interactions with bacterial targets.

The halogen-substituted derivatives **(4g)** (4-Cl), **(4h)** (2-Cl), and **(4i)** (4-Br) also displayed significant antibacterial activity. Notably, compound **(4i)** exhibited MIC values of 25 µg/mL against *S. aureus* and *S. pyogenes*, indicating excellent activity toward Gram-positive organisms. The activity trend among halogenated derivatives followed the order: **F > Br > Cl** suggesting that both the electronic nature and size of the substituent influence antibacterial performance. The superior activity of the fluoro derivative may be associated with the unique ability of fluorine to enhance lipophilicity, metabolic stability, and target-binding affinity without introducing significant steric hindrance.

Heteroaromatic derivatives **(4n)** (3-pyridyl) and **(4p)** (2-thienyl) exhibited good antibacterial activity with MIC values of 50-62.5 µg/mL against most tested organisms. The presence of heteroatoms within these aromatic systems may facilitate additional hydrogen-bonding and dipolar interactions with biological targets, thereby contributing to enhanced antimicrobial activity. Similarly, the furyl derivative **(4o)** displayed moderate activity, although slightly lower than its pyridyl and thienyl counterparts.

In contrast, compounds containing electron-donating substituents generally showed reduced antibacterial potency. The methoxy-substituted derivatives **(4b)**, **(4f)**, **(4j)**, and **(4k)**, as well as the methyl-substituted analogues **(4c)** and **(4d)**, exhibited MIC values predominantly within the range of 125-250 µg/mL. Among these compounds, the *ortho*-methyl derivative **(4d)** was less active than the *para*-methyl analogue **(4c)**, indicating that steric hindrance near the reaction center adversely affects biological activity. The dimethylamino-substituted derivative **(4e)** was the least active member of the series, displaying MIC values of 200-250 µg/mL against all tested strains. The strong electron-donating character of the dimethylamino group likely reduces the electrophilic character of the aromatic ring and diminishes favorable interactions with bacterial targets. Comparison of the unsubstituted phenyl derivative **(4a)** with substituted analogues further confirms the beneficial effect of electron-withdrawing groups. While compound **(4a)** exhibited only moderate activity (MIC = 100-125 µg/mL), introduction of fluoro, bromo, chloro, or nitro substituents significantly enhanced antibacterial potency, emphasizing the critical role of electronic effects in governing biological activity.

Interestingly, Gram-positive bacteria were generally more susceptible to the synthesized compounds than Gram-negative bacteria. This behaviour can be attributed to the additional outer lipopolysaccharide membrane present in Gram-negative organisms, which restricts penetration of antimicrobial agents. Nevertheless, compounds **(4l)**, **(4m)**, and **(4i)** retained excellent activity against both bacterial classes, highlighting their broad-spectrum antibacterial potential.

The observed antibacterial profile demonstrates that molecular hybridization of the biologically privileged trifluoromethyl coumarin scaffold with the 4*H*-pyran pharmacophore generates highly promising antimicrobial agents. In particular, the presence of electron-withdrawing substituents such as fluorine, nitro, bromine, and chlorine significantly enhances antibacterial efficacy. Among the synthesized series, compounds **(4l)**, **(4m)**, and **(4i)** emerged as the most potent candidates and may serve as valuable lead molecules for further optimization and mechanistic investigation aimed at developing new fluorinated antibacterial agents.

3.5.2. In vitro antifungal activity

The synthesized trifluoromethyl coumarin-based 4*H*-pyran derivatives **(4a-p)** were evaluated for their *in vitro* antifungal activity against *Candida albicans* (MTCC 227), *Aspergillus niger* (MTCC 282), and *Aspergillus clavatus* (MTCC 1323). The minimum inhibitory concentration (MIC) values are summarized in **Table 7**. MIC values reported in **Tables 7** represent the modal MIC obtained from three independent experiments. Replicate assays produced identical or highly consistent MIC values, indicating good reproducibility of the antifungal evaluation. Nystatin and griseofulvin were used as reference antifungal drugs for comparison. The antifungal screening results revealed that the synthesized compounds exhibited a broad range of activity, with MIC values varying from 62.5 to 1000 µg/mL **(Fig. 7)**. A clear structure-activity relationship was observed, indicating that the antifungal potency was strongly influenced by the electronic nature and position of the substituents attached to the aryl ring of the pyranochromene framework.

Among all compounds tested, the *para*-fluoro derivative **(4l)** emerged as the most potent antifungal agent of the series. Compound **(4l)** displayed MIC values of 62.5 µg/mL against both *C. albicans* and *A. niger*, and 100 µg/mL against *A. clavatus*. Notably, its activity against *C. albicans* was superior to both reference drugs, Nystatin (100 µg/mL) and griseofulvin (500 µg/mL). The enhanced activity of **(4l)** may be attributed to the unique physicochemical properties of fluorine, which can improve lipophilicity, membrane permeability, metabolic stability, and target-binding affinity. The halogenated derivatives **(4g)** (4-Cl), **(4h)** (2-Cl), and **(4i)** (4-Br) also demonstrated significant antifungal activity. Compound **(4i)** exhibited MIC values of 100 µg/mL against all three fungal strains, while compound **(4g)** showed identical activity across the tested fungi. The *ortho*-chloro derivative **(4h)** displayed slightly reduced activity against *C. albicans* but retained good potency against both *Aspergillus* species. These findings suggest that halogen substitution plays an important role in enhancing antifungal activity, likely through increased hydrophobic interactions with fungal cell membranes. The nitro-substituted derivative **(4m)** also exhibited noteworthy antifungal activity, with MIC values of 100 µg/mL against *C. albicans* and *A. niger* and 125 µg/mL against *A. clavatus*. Although slightly less active than the fluoro analogue **(4l)**, the presence of

the strongly electron-withdrawing nitro group clearly contributes to enhanced fungal growth inhibition. The overall activity trend among the electron-withdrawing derivatives can be approximated as: **4-F > 4-Br ≈ 4-Cl ≈ 4-NO_2**, indicating that fluorine substitution provides the most favorable balance of electronic and steric effects for antifungal activity within this series.

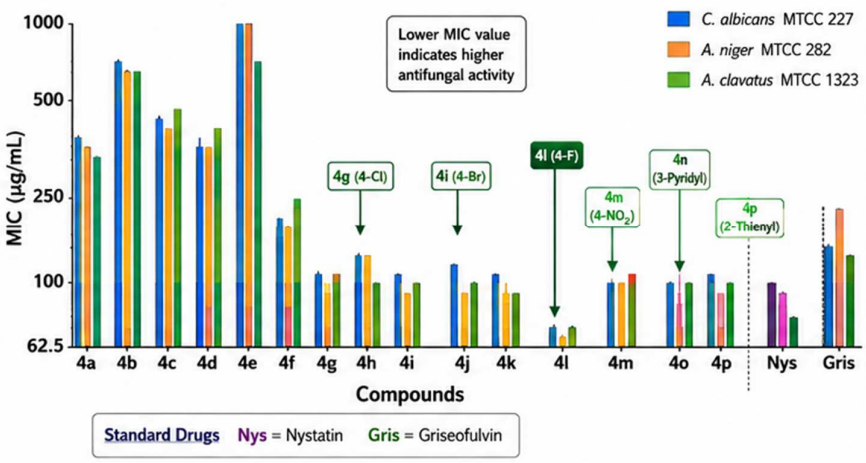

Fig. 7. Antifungal activity of trifluoromethyl coumarin-based 4*H*-pyran derivatives **(4a-p)**

Table 7. *In vitro* antifungal activity[a] of trifluoromethyl coumarin-based 4*H*-pyran derivatives **(4a-p)**

Compound Code	R	MIC [µg/mL]		
		C. Albicans MTCC 227	A. *Niger* MTCC 282	*A. Clavatus MTCC 1323*
(4a)	C_6H_5	250	250	250
(4b)	4-OCH_3-C_6H_4	500	500	250
(4c)	4-CH_3-C_6H_4	500	250	250
(4d)	2-CH_3-C_6H_4	500	500	500
(4e)	4-$N(CH_3)_2$-C_6H_4	1000	500	500
(4f)	3-OCH_3-C_6H_4	500	250	250
(4g)	4-Cl-C_6H_4	100	100	100
(4h)	2-Cl-C_6H_4	250	100	100
(4i)	4-Br-C_6H_4	100	100	100
(4j)	2,5-diOMe-C_6H_3	500	500	250
(4k)	3,4,5-triOMe-C_6H_2	500	500	500
(4l)	4-F-C_6H_4	62.5	62.5	100
(4m)	4-NO_2-C_6H_4	100	100	125
(4n)	3-Pyridyl	100	100	100
(4o)	2-Furyl	250	100	125
(4p)	2-Thienyl	100	100	125
Nystatin		100	100	100
Greseofulvin		500	100	100

[a] = Values represent the mean of three independent experiments (n = 3). DMSO (≤1%, v/v) showed no inhibitory effect on microbial growth. Statistical significance was evaluated by one-way ANOVA followed by Tukey's multiple comparison tests ($p < 0.05$).

The heteroaromatic derivatives **(4n)** (3-pyridyl) and **(4p)** (2-thienyl) exhibited good antifungal activity with MIC values of 100-125 µg/mL, comparable to those of Nystatin against several fungal strains. The pyridyl ring may contribute additional hydrogen-bonding interactions, whereas the thienyl moiety can enhance lipophilic contacts with fungal targets. Similarly, the furyl derivative **(4o)** displayed moderate activity, particularly against *A. niger*. In contrast, compounds containing electron-donating substituents generally exhibited significantly lower antifungal activity. The methoxy-substituted derivatives **(4b)**, **(4f)**, **(4j)**, and **(4k)**, as well as the methyl-substituted compounds **(4c)** and **(4d)**, displayed MIC values

predominantly in the range of 250-500 µg/mL. The dimethylamino derivative **(4e)** was the least active compound of the series, showing MIC values of 500-1000 µg/mL against the tested fungal strains. The reduced activity of these compounds suggests that strong electron-donating substituents diminish favourable interactions with fungal targets and adversely affect the antifungal profile.

Comparison of the unsubstituted phenyl analogue **(4a)** with substituted derivatives further highlights the importance of electronic effects. While compound **(4a)** exhibited only moderate activity (MIC = 250 µg/mL), incorporation of fluorine, bromine, chlorine, nitro, or heteroaromatic substituents substantially improved antifungal potency. These observations indicate that electron-withdrawing and heteroaromatic functionalities are beneficial for antifungal activity within this molecular framework.

Overall, the antifungal evaluation demonstrates that molecular hybridization of the trifluoromethyl coumarin nucleus with the 4*H*-pyran scaffold generates compounds with promising antifungal properties. The presence of fluorinated and halogenated substituents significantly enhances activity, with compound **(4l)** emerging as the most potent antifungal candidate of the series. The superior performance of **(4l)**, together with the favorable activities of compounds **(4g)**, **(4i)**, **(4m)**, **(4n)**, and **(4p)**, identifies these derivatives as attractive lead structures for further optimization and development of new fluorinated antifungal agents.

3.6. Structure-activity relationship (SAR) study

A comparative analysis of the antibacterial and antifungal activities of the synthesized trifluoromethyl coumarin-based 4H-pyran derivatives **(4a-p)** revealed that the antimicrobial profile within the present series was influenced by the electronic nature, substitution pattern, and structural characteristics of the aryl or heteroaryl group attached to the pyranochromene nucleus **(Fig. 8).** The observed SAR trends are discussed specifically for the synthesized derivatives evaluated in the present study and should not be considered as generalized relationships applicable to all trifluoromethyl coumarin-based 4*H*-pyran analogues.

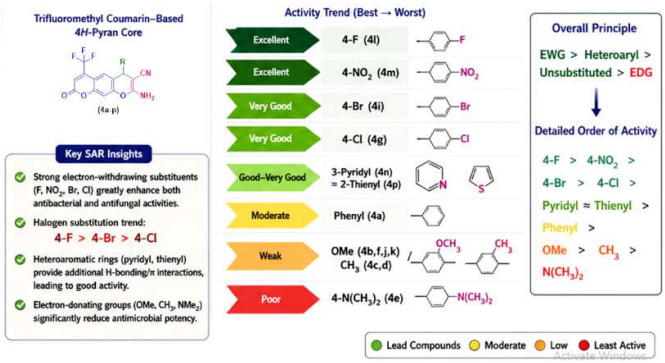

Fig. 8. SAR study of trifluoromethyl coumarin-based 4*H*-pyran derivatives **(4a-p)**

The unsubstituted phenyl derivative **(4a)** showed moderate antibacterial activity, with MIC values of 100-125 µg/mL, and moderate antifungal activity, with MIC values of 250 µg/mL against all three fungal strains. Modification of the phenyl ring produced substantial changes in antimicrobial potency. Within the synthesized series, derivatives containing electron-withdrawing substituents, particularly halogen and nitro groups, generally exhibited improved antibacterial and antifungal activities compared with the unsubstituted analogue (4a). This trend was most evident for the *para*-fluoro **(4l)**, *para*-nitro **(4m)**, *para*-bromo **(4i)**, and *para*-chloro **(4g)** derivatives.

Among the synthesized compounds, the *para*-fluoro derivative **(4l)** exhibited the most favorable overall antimicrobial profile. It showed antibacterial MIC values of 25-50 µg/mL against the tested bacterial strains and antifungal MIC values of 62.5-100 µg/mL. The *para*-nitro derivative **(4m)** also demonstrated strong antibacterial activity, with MIC values of 25-62.5 µg/mL, together with good antifungal activity (100-125 µg/mL). The *para*-bromo derivative **(4i)** exhibited particularly strong activity against the Gram-positive bacteria, with MIC values of 25 µg/mL against both *S. aureus* and *S. pyogenes*, while the *para*-chloro analogue **(4g)** displayed MIC values of 50-62.5 µg/mL against the tested bacteria. These results indicate that, within the present compound series, the incorporation of selected electron-withdrawing substituents was associated with enhanced antimicrobial activity.

The positional effect of halogen substitution was also apparent. Comparison of the *para*-chloro derivative **(4g)** with its *ortho*-chloro analogue **(4h)** showed that the para-substituted compound was more active against both bacterial and fungal strains. Similarly, the *para*-bromo derivative **(4i)** exhibited stronger antibacterial activity than the *para*-chloro analogue **(4g)**, particularly against Gram-positive bacteria. These observations suggest that both the electronic characteristics and substitution position of the halogen may influence antimicrobial activity within the present series. However, the available data do not support assigning a universal halogen activity order, as the relative potency varied depending on the microorganism evaluated.

The electron-donating substituents generally resulted in lower antimicrobial activity within the synthesized series. The methoxy-containing derivatives **(4b)**, **(4f)**, **(4j)**, and **(4k)**, together with the methyl-substituted compounds **(4c)** and **(4d)**, showed predominantly moderate to weak antibacterial and antifungal activities. The *para*-methoxy derivative **(4b)** and meta-methoxy derivative **(4f)** exhibited antibacterial MIC values of 125-250 µg/mL and antifungal MIC values of 250-500 µg/mL. The dimethoxy- and trimethoxy-substituted derivatives **(4j)** and **(4k)** similarly displayed reduced activity compared with the halogenated and nitro-substituted analogues. Notably, the dimethylamino derivative **(4e)** was among the least active compounds, with antibacterial MIC values of 200-250 µg/mL and antifungal MIC values of 500-1000 µg/mL. Thus, for the compounds investigated herein, strongly electron-donating substituents were generally associated with reduced antimicrobial potency.

The influence of substituent position was further illustrated by comparison of the methyl-substituted derivatives. The *ortho*-methyl analogue **(4d)** exhibited lower antibacterial and antifungal activity than the corresponding *para*-methyl derivative **(4c)**. This difference may be related to the steric influence of the *ortho* substituent, which could affect the preferred molecular conformation or the accessibility of the pharmacophoric framework. A similar positional effect was observed for the chloro derivatives, where the *para*-chloro compound **(4g)** was more active than the *ortho*-chloro analogue **(4h)**. These comparisons indicate that the position of substitution, in addition to its electronic character, may contribute to the observed antimicrobial profile of the synthesized derivatives. The heteroaryl derivatives **(4n-p)** also displayed noteworthy antimicrobial activity. The 3-pyridyl derivative **(4n)** and 2-thienyl derivative **(4p)** exhibited antibacterial MIC values of 50-62.5 µg/mL and antifungal MIC values predominantly of 100-125 µg/mL. The 2-furyl derivative **(4o)** showed comparatively moderate activity, with antibacterial MIC values of 62.5-100 µg/mL and antifungal MIC values of 100-250 µg/mL. The improved activity observed for some heteroaryl derivatives may be associated with the additional heteroatoms and altered electronic and physicochemical properties of these substituents, which could influence molecular interactions with microbial targets. Nevertheless, the present data do not permit a definitive assignment of a specific mechanism for these effects.

Overall, the antimicrobial results indicate that the biological activity of the synthesized trifluoromethyl coumarin-based 4*H*-pyran derivatives is sensitive to the nature and position of the substituent attached to the pyranochromene framework. Within the series investigated herein, compounds bearing selected electron-withdrawing substituents, particularly 4-F **(4l)**, 4-NO_2 **(4m)**, 4-Br **(4i)**, and 4-Cl **(4g)**, generally exhibited improved antimicrobial activity relative to the unsubstituted phenyl derivative **(4a)**, whereas electron-donating substituents were generally associated with lower activity. Among the synthesized compounds, **(4l)** showed the most balanced antibacterial and antifungal profile and can therefore be considered a promising lead for further investigation. Compounds (4m), (4i), **(4g)**, and the heteroaryl derivative **(4n)** also demonstrated noteworthy antimicrobial activity against selected microorganisms.

Importantly, these SAR observations represent trends identified within the synthesized derivatives evaluated in the present study and should not be generalized beyond this compound series without further experimental validation. The limited number of previously reported trifluoromethyl coumarin-based 4*H*-pyran hybrids further emphasizes the originality of the present work. The present findings provide an initial SAR framework for this relatively underexplored class of hybrid molecules and may serve as a basis for future structural optimization, mechanistic investigations, and molecular modeling studies aimed at developing more potent antimicrobial derivatives.

4. Conclusion

In summary, an efficient, rapid, and environmentally benign microwave-assisted one-pot protocol has been developed for the synthesis of novel trifluoromethyl coumarin-based 4*H*-pyran hybrids using freshly extracted lemon juice as a green bio-catalyst. The methodology afforded a diverse library of pyrano[3,2-*g*]chromene derivatives **(4a-p)** in excellent yields (86-94%) within 4-8 min under optimized conditions. The catalyst system demonstrated excellent catalytic efficiency, operational simplicity, and recyclability, highlighting its potential as a sustainable alternative to conventional catalytic methods. Biological evaluation identified several compounds with significant antibacterial and antifungal activities, with derivatives **(4l)**, **(4m)**, and **(4i)** emerging as the most potent analogues. Structure-activity relationship studies revealed that electron-withdrawing substituents on the aryl ring play a crucial role in enhancing antimicrobial potency. Overall, this work demonstrates that the integration of trifluoromethyl coumarin and 4*H*-pyran pharmacophores through a green synthetic strategy provides an effective platform for the development of bioactive fluorinated heterocycles. The promising antimicrobial profiles of compounds **(4l)**, **(4m)**, and **(4i)** warrant further investigation as potential lead candidates for the development of new antimicrobial agents.

Acknowledgment

The authors express their sincere gratitude to Gujarat Fluorochemicals Ltd. & Microcare Laboratory and TRC for providing the support for this research

References

1. Kohansal M. (2025) Advances in green chemistry: Sustainable approaches in organic synthesis. *Int. J. New Chem.*, *12*, 4.
2. Chiang P.-C., Ma H.-W., Wen L., Lin C.-H. (2024) Application of green chemistry principles to green economy. In: *Introduction to Green Science and Technology for Green Economy: Principles and Applications*. Springer, pp. 287-333.

3. Bisharat H., Javaid S., Ahmad Z., Mahmood S., Saeed A., Khan D. (2026) Recent advances in green catalytic multicomponent reactions for sustainable synthesis. *ChemistrySelect*, *11*, e06024.
4. Delost M.D., Smith D.T., Anderson B.J., Njardarson J.T. (2018) From oxiranes to oligomers: Architectures of US FDA approved pharmaceuticals containing oxygen heterocycles. *J. Med. Chem.*, *61*, 10996-11020.
5. El-Bana G.G., Salem M.A., Helal M.H., Alharbi O., Gouda M.A. (2024) A review on the recent multicomponent synthesis of 4*H*-pyran derivatives. *Mini Rev. Med. Chem.*, *21*, 73-91.
6. Hatakeyama S., Ochi N., Numata H., Takano S. (1988) A new route to substituted 3-methoxycarbonyldihydropyrans; enantioselective synthesis of (−)-methyl elenolate. *Chem. Commun.*, 1202-1204.
7. Singh K., Singh J., Singh H. (1996) A synthetic entry into fused pyran derivatives through carbon transfer reactions of 1,3-oxazinanes and oxazolidines with carbon nucleophiles. *Tetrahedron*, *52*, 14273-14280.
8. Kumar D., Singh G., Sharma P., Qayum A., Mahajan G., Mintoo M., Singh S.K., Mondhe D.M., Bedi P., Jain S.K. (2018) 4-Aryl/heteroaryl-4*H*-fused pyrans as anti-proliferative agents: Design, synthesis and biological evaluation. *Anti-Cancer Agents Med. Chem.*, *18*, 57-73.
9. Nazari P., Bazi A., Ayatollahi S.A., Dolati H., Mahdavi S.M., Rafighdoost L., Amirmostofian M. (2017) Synthesis and evaluation of the antimicrobial activity of spiro-4*H*-pyran derivatives on some Gram-positive and Gram-negative bacteria. *Iran. J. Pharm. Res.*, *16*, 943.
10. Kumar R.S., Almansour A.I., Arumugam N., Al-Thamili D.M., Basiri A., Kotresha D., Manohar T.S., Venketesh S., Asad M., Asiri A.M. (2018) Highly functionalized 2-amino-4*H*-pyrans as potent cholinesterase inhibitors. *Bioorg. Chem.*, *81*, 134-143.
11. He M.T., Kim S.J., Le V.D., Min S.J., Lee H., Lee J.W., Shin M.-S. (2025) Novel pyran-based anti-inflammatory agents: Design, synthesis, and mechanistic studies in LPS-stimulated macrophages. *Appl. Biol. Chem.*, *68*, 47.
12. El-Sayed N.N., Zaki M.E., Al-Hussain S.A., Ben Bacha A., Berredjem M., Masand V.H., Almarhoon Z.M., Omar H.S. (2022) Synthesis and evaluation of some new 4*H*-pyran derivatives as antioxidant, antibacterial and anti-HCT-116 cells of CRC, with molecular docking, antiproliferative, apoptotic and ADME investigations. *Pharmaceuticals*, *15*, 891.
13. Mahdavi S.M., Habibi A., Dolati H., Shahcheragh S.M., Sardari S., Azerang P. (2018) Synthesis and antimicrobial evaluation of 4*H*-pyrans and Schiff base fused 4*H*-pyran derivatives as inhibitors of *Mycobacterium bovis* (BCG). *Iran. J. Pharm. Res.*, *17*, 1229.
14. Nath R., Ashique S., Nehra B., Debnath I., Ghosh S., Chawla P.A., Al-Salem F.M., Yasmin S., Hussain M.S., Das L. (2026) Rational drug design and synthesis of novel bioactive molecules with oxygen heterocycles, including AChE and BChE inhibitory properties and SAR studies. *Mol. Divers.*, 1-53.
15. Chioua M., Pérez-Peña J., García-Font N., Moraleda I., Iriepa I., Soriano E., Marco-Contelles J., Oset-Gasque M.J. (2015) Pyranopyrazolotacrines as nonneurotoxic, Aβ-anti-aggregating and neuroprotective agents for Alzheimer's disease. *Future Med. Chem.*, *7*, 845-855.
16. Pourshojaei Y., Abiri A., Eskandari R., Dourandish F., Eskandari K., Asadipour A. (2019) Synthesis, biological evaluation, and computational studies of novel fused six-membered O-containing heterocycles as potential acetylcholinesterase inhibitors. *Comput. Biol. Chem.*, *80*, 249-258.
17. Vanam R., Allam V., Nerella S., Gavaji B. (2021) Green synthesis of chromene congeners via multi-component reaction and their antimicrobial studies. *ChemistrySelect*, *6*, 9591-9598.
18. Borah B., Dwivedi K.D., Chowhan L.R. (2022) Review on synthesis and medicinal application of dihydropyrano[3,2-*b*]pyrans and spiro-pyrano[3,2-*b*]pyrans by employing the reactivity of 5-hydroxy-2-(hydroxymethyl)-4*H*-pyran-4-one. *Polycycl. Aromat. Comp.*, *42*, 5893-5937.
19. Samai S., Atta S., Singh M.S. (2025) Synthetic strategies toward 2*H*-, 4*H*-pyrans, and pyranones: Recent advances. *ChemistrySelect*, 10, e01023.
20. Venkatachalam H., Kumar N.V.A. (2019) The oxygen-containing fused heterocyclic compounds. In: *Heterocycles-Synthesis and Biological Activities*. IntechOpen.
21. Vekariya R.H., Patel H.D. (2014) Recent advances in the synthesis of coumarin derivatives via Knoevenagel condensation: A review. *Synth. Commun.*, *44*, 2756-2788.
22. Cheke R.S., Patel H.M., Patil V.M., Ansari I.A., Ambhore J.P., Shinde S.D., Kadri A., Snoussi M., Adnan M., Kharkar P.S. (2022) Molecular insights into coumarin analogues as antimicrobial agents: Recent developments in drug discovery. *Antibiotics*, *11*, 566.
23. Vekariya R.H., Patel K.D., Rajani D.P., Rajani S.D., Patel H.D. (2017) A one pot, three component synthesis of coumarin hybrid thiosemicarbazone derivatives and their antimicrobial evaluation. *J. Assoc. Arab Univ. Basic Appl. Sci.*, *23*, 10-19.
24. Lončar M., Gašo-Sokač D., Molnar M. (2023) Coumarin derivatives as antifungal agents-A review. *Czech J. Food Sci.*, 41, 2.
25. Prusty J.S., Kumar A. (2020) Coumarins: Antifungal effectiveness and future therapeutic scope. *Mol. Divers.*, *24*, 1367-1383.
26. Mishra S., Pandey A., Manvati S. (2020) Coumarin: An emerging antiviral agent. *Heliyon*, 6, e03217.
27. Rawat A., Reddy A.V.B. (2022) Recent advances on anticancer activity of coumarin derivatives. *Eur. J. Med. Chem. Rep.*, *5*, 100038.
28. Ramsis T.M., Ebrahim M.A., Fayed E.A. (2023) Synthetic coumarin derivatives with anticoagulation and antiplatelet aggregation inhibitory effects. *Med. Chem. Res.*, *32*, 2269-2278.

29. Fylaktakidou K.C., Hadjipavlou-Litina D.J., Litinas K.E., Nicolaides D.N. (2004) Natural and synthetic coumarin derivatives with anti-inflammatory/antioxidant activities. *Curr. Pharm. Des.*, *10*, 3813-3833.
30. Hu X.-L., Gao C., Xu Z., Liu M.-L., Feng L.-S., Zhang G.-D. (2018) Recent development of coumarin derivatives as potential antiplasmodial and antimalarial agents. *Curr. Top. Med. Chem.*, *18*, 114-123.
31. Hu Y.-Q., Xu Z., Zhang S., Wu X., Ding J.-W., Lv Z.-S., Feng L.-S. (2017) Recent developments of coumarin-containing derivatives and their anti-tubercular activity. *Eur. J. Med. Chem.*, *136*, 122-130.
32. Bansal Y., Sethi P., Bansal G. (2013) Coumarin: A potential nucleus for anti-inflammatory molecules. *Med. Chem. Res.*, *22*, 3049-3060.
33. Annunziata F., Pinna C., Dallavalle S., Tamborini L., Pinto A. (2020) An overview of coumarin as a versatile and readily accessible scaffold with broad-ranging biological activities. *Int. J. Mol. Sci.*, *21*, 4618.
34. Meanwell N.A. (2018) Fluorine and fluorinated motifs in the design and application of bioisosteres for drug design. *J. Med. Chem.*, *61*, 5822-5880.
35. Patil V., Nitave S., Dhulasavant V., Latwade R. (2025) The future of precision medicine: Exploring fluorinated building blocks for targeted drug design. *J. Appl. Chem. Sci. Int.*, *16*, 143-156.
36. Novás M., Matos M.J. (2025) The role of trifluoromethyl and trifluoromethoxy groups in medicinal chemistry: Implications for drug design. *Molecules*, *30*, 3009.
37. Chaudhari S.B., Kumar A., Mankar V.H., Banerjee S., Kumar D., Mubarak N.M., Dehghani M.H. (2024) Diverse role, structural trends, and applications of fluorinated sulphonamide compounds in agrochemical and pharmaceutical fields. *Heliyon*, *10*, e32409.
38. Nair A.S., Singh A.K., Kumar A., Kumar S., Sukumaran S., Koyiparambath V.P., Pappachen L.K., Rangarajan T., Kim H., Mathew B. (2022) FDA-approved trifluoromethyl group-containing drugs: A review of 20 years. *Processes*, 10, 2054.
39. Detsi A., Kontogiorgis C., Hadjipavlou-Litina D. (2017) Coumarin derivatives: An updated patent review (2015-2016). *Expert Opin. Ther. Pat.*, *27*, 1201-1226.
40. Citarella A., Vittorio S., Dank C., Ielo L. (2024) Syntheses, reactivity, and biological applications of coumarins. *Front. Chem.*, *12*, 1362992.
41. de Sena Murteira Pinheiro P., Franco L.S., Montagnoli T.L., Fraga C.A.M. (2024) Molecular hybridization: A powerful tool for multitarget drug discovery. *Expert Opin. Drug Discov.*, *19*, 451-470.
42. Kumar S., Arora A., Kumar S., Kumar R., Senapati N.N., Singh B.K. (2025) Pyran-fused analogues and their potential applications. *Russ. J. Bioorg. Chem.*, *51*, 373-438.
43. Helal M.H., Alrashdi S., Alsharif H., Moussa Z., Elgammal W.E., Halawa A.H., Elhenawy A.A., El-Agrody A.M. (2025) Targeting P-glycoprotein with novel halogenated 4*H*-pyran-coumarin hybrids: A combined experimental and computational approach to tumor-sensitive and resistant breast cancer cell lines. *J. Biomol. Struct. Dyn.*, 1-20.
44. Pasricha S., Mittal K., Gahlot P., Kaur H., Avasthi N., Shweta. (2022) Multicomponent synthetic strategies and perspectives for synthesis of linked or fused coumarin heterocycles. *J. Iran. Chem. Soc.*, *19*, 4035-4092.
45. Ye R., Zhao J., Wickemeyer B.B., Toste F.D., Somorjai G.A. (2018) Foundations and strategies of the construction of hybrid catalysts for optimized performances. *Nat. Catal.*, *1*, 318-325.
46. Pal R. (2013) Fruit juice: A natural, green and biocatalyst system in organic synthesis. *Open J. Org. Chem.*, 1, 47-56.
47. Kumar V., Saha R., Chatterjee S., Mishra V. (2023) From traditional to greener alternatives: Potential of plant resources as a biotransformation tool in organic synthesis. *React. Chem. Eng.*, *8*, 2677-2688.
48. Khan R.A., Adole V.A., Pawar T.B., Jagdale B.S. (2024) Green chemistry approach to the synthesis of 2-aryl/heteroaryl substituted 2,3-dihydroquinazolin-4(1H)-ones using lemon juice under concentrated solar radiations as a renewable source. *RSC Adv.*, *14*, 32350-32357.
49. Vekariya R.H., Patel K.D., Patel H.D. (2016) Fruit juice of *Citrus limon* as a biodegradable and reusable catalyst for facile, eco-friendly and green synthesis of 3,4-disubstituted isoxazol-5(4*H*)-ones and dihydropyrano[2,3-*c*]pyrazole derivatives. *Res. Chem. Intermed.*, *42*, 7559-7579.
50. Wu J., Diao T., Sun W., Li Y. (2006) Expeditious approach to coumarins via Pechmann reaction catalyzed by molecular iodine or AgOTf. *Synth. Commun.*, *36*, 2949-2956.
51. Chandrasekaran M., Venkatesalu V. (2004) Antibacterial and antifungal activity of Syzygium jambolanum seeds. *J. Ethnopharmacol.*, 91, 105-108.
52. Tajane S.B., Pawar S., Mohite S.T., Patil S.R. (2024) Comparative analysis of in-house and commercially available media for determining the antifungal susceptibility profile of Candida species. *Drugs Drug Candidates*, *4*, 5.
53. Desai N.C., Pandya D.D., Kotadiya G.M., Desai P. (2013) Synthesis of pyridyl benzimidazoles encompassing 4-thiazolidinone derivatives as potential antimicrobial agents. *Lett. Drug Des. Discov.*, *10*, 942-950.

© 2026 by the authors; licensee Growing Science, Canada. This is an open access article distributed under the terms and conditions of the Creative Commons Attribution (CC-BY) license (http://creativecommons.org/licenses/by/4.0/).